

## GRAVITATIONAL INTERACTION OF TWO PLANETESIMALS MOVING IN CLOSE ORBITS

S. I. Ipatov

UDC 523.52:521.131

*Studies of the orbital evolution of two gravitationally interacting material-point objects moving around the sun are reported. The work was done basically by numerical integration of the plane three-body problem. The following types of orbital evolution were considered: motion about triangular libration points on tadpole and horseshoe synodic orbits (types M and N), the case of close approaches of the objects (type A), and chaotic variations of the orbital elements during which close approaches of the objects are impossible (type C). In the case of initially circular orbits with an initial angle  $\varphi_0 = 60^\circ$  between the lines to the objects from the sun vertex and  $10^{-9} \leq \mu \leq 2 \cdot 10^{-4}$ , the maximum values of  $\varepsilon_0 = (a_2^0 - a_1^0)/a_1^0$  that correspond to types N, M, A, and C were found to be equal respectively to  $\alpha = 1.63-1.64\mu^{1/2}$ ,  $\beta = 0.77-0.81\mu^{1/3}$ ,  $\gamma = 2.1-2.45\mu^{1/3}$  and  $\delta = 1.45-1.64\mu^{2/7}$ , where  $a_1^0$  and  $a_2^0$  are the initial values of the semimajor axes and  $\mu$  is the ratio of the sum of the masses of the objects to the mass of the sun. The values of  $\alpha$ ,  $\beta$ , and  $\delta$  are generally smaller for other values of  $\varphi_0$ . When  $\varepsilon_0 = 0$ , the smallest values of  $\varphi_0$ , which correspond to types N and M, are near 0.4 and  $0.4\mu^{1/3}$  rad. The maximum eccentricities at  $\mu_1 \leq 10^{-5}$  did not usually exceed  $(7-8) \cdot \mu_1^{1/3}$  for type A or  $(4-6) \cdot \mu_1^{1/3}$  for type C, where  $\mu_1$  is the mass of the larger object in sun masses.*

### INTRODUCTION

Many recent publications [2-4, 7-8, 10-12, 14, 16-48 and others] have reported studies of the orbital evolution of two gravitationally interacting bodies moving around a massive center on close orbits. One type of interaction between such objects is motion about triangular libration points. Examples of objects that move about these points in the present solar system are the Trojans of Jupiter and the analogous Trojans of other planets (e.g., the asteroid 1990 MB, which is a "Martian Trojan" [35]), and the Saturnian satellites Janus (1980 S1) and Epimethe (1980 S3), Dione and Elena (1980 S6), Tethys, Telesto (1980 S13) and Calypso (1980 S25), which are in 1:1 resonance with one another [13, 23].

Study of the evolution of intersecting orbits enables us to estimate the mutual gravitational influence of bodies of the asteroid and transneptunian belts and the possibility of their migration toward planet orbits. Over a certain interval of time, several bodies migrating in the solar system can cross the orbit of only one of the planets, and their interaction with that planet can be treated within the framework of a three-body problem. For example, certain asteroids cross only the orbit of Mars or only that of the earth.

Studies of the interaction of two close planetesimals, an elementary process in a protoplanetary disk, lead to better understanding of the evolution of the disk and enable us to estimate protoplanet feeding zones and the influence of planetesimals on the orbital evolution of nearby smaller objects. These studies have also been used to estimate planetary accretion rates [25, 26] and the origin of their axial rotations [5-6, 11, 33, 43]. On the basis of such studies we plan to develop an algorithm for approximate calculation of the gravitational interactions of planetesimals in a disk composed of a large number of objects.

This paper reports studies of the interactions of two material-point (MP) objects moving around a massive central body (sun) on initially close orbits. The mutual gravitational effects of the MPs were taken into account by numerical integration of the equations of motion.

When the orbits of the two gravitationally interacting MPs were initially circular, we adjusted the boundaries of the initial-data ranges that correspond to various types of orbital-element variations. The range of masses of the larger MP was varied from  $10^{-9}$  to  $10^{-3}$  of the mass of the gravitating center. The case of identical MPs and the dependence of

---

Institute of Applied Mathematics, Russian Academy of Sciences. Translated from *Astronomicheskii Vestnik*, Vol. 28, No. 6, pp. 10-33, November-December, 1994. Original article submitted March 24, 1994; revision submitted June 2, 1994.

TABLE 1. Boundaries of Ranges of  $\varepsilon_0 = (a_2^0 - a_1^0)/a_1^0$  Corresponding to Various Evolutionary Types  $N_t$  for  $e_1^0 = e_2^0 = 0$ ,  $\varphi_0 = 60^\circ$  and  $T_0 = 2500$

$N_t$	$10^{-3}$	$10^{-4}$	$10^{-5}$	$10^{-6}$	$10^{-7}$	$10^{-8}$	$10^{-9}$
$\mu_2$	$10^{-7}$	$10^{-6}$	$10^{-7}$	$10^{-8}$	$10^{-9}$	$10^{-10}$	$10^{-11}$
$\delta_\mu$	0,285	0,105	0,0546	0,0286	0,0151	0,00745	0,00390
$\delta_t$	0,284	0,104	0,0545	0,0285	0,0150	0,00740	0,00389
$\gamma_w$	0,234	0,105	0,0530	0,0230	0,0108	0,00460	0,00186
$\gamma_t$	0,233	0,104	0,0525	0,0225	0,0107	0,00455	0,00185
$\beta_w$	0,0541	0,0351	0,0172	0,0081	0,00393	0,00194	0,00101
$\beta_t$	0,0540	0,0350	0,0171	0,0080	0,00392	0,00193	0,001
$\alpha_\mu$	—	0,0167	0,00522	0,00165	0,000520	0,000165	—
$\alpha_t$	—	0,0166	0,00521	0,00164	0,000519	0,000164	—
$\delta/\mu^{1/4}$	1,60	1,04	0,97	0,90	0,85	0,74	0,69
$\delta/\mu^{2/7}$	2,05	1,45	1,46	1,47	1,50	1,43	1,45
$\delta/\mu^{1/3}$	2,915	2,24	2,52	2,85	3,23	3,43	3,88
$\gamma/\mu^{1/3}$	2,33	2,24	2,44	2,27	2,31	2,12	1,85
$\gamma/h$	3,37	3,24	3,52	3,27	3,33	3,05	2,67
$\beta/\mu^{1/4}$	0,30	0,35	0,30	0,25	0,22	0,19	0,18
$\beta/\mu^{1/3}$	0,54	0,75	0,79	0,80	0,84	0,90	1,0
$\beta/h$	0,78	1,09	1,14	1,16	1,22	1,29	1,44
$\alpha/\mu^{1/3}$	—	0,36	0,24	0,16	0,11	0,076	—
$\alpha/\mu^{1/2}$	—	1,66	1,64	1,64	1,63	1,64	—
$\Delta C$	0,18	0	0,03	0,20	0,29	0,38	0,52
$\Delta A$	0,63	0,66	0,65	0,52	0,45	0,36	0,22
$\Delta M$	0	0,18	0,22	0,22	0,23	0,24	0,25
$\Delta N$	0,19	0,16	0,10	0,06	0,03	0,02	0,01

the above ranges on the initial angle between the lines to the MPs are discussed here for the first time; we also determine the maximum eccentricities and ranges of variation of the distances of the MPs from the sun for those types. Several cases of initially eccentric orbits are investigated.

### VARIANT CALCULATIONS

Studies of the orbital evolution of two gravitationally interacting MP objects moving around a massive central body (sun) in the same plane were based on numerical integration of the equations of motion of the plane three-body problem. About a thousand pairs of MPs were considered. The calculations were made on a 48-place BESM-6 computer, which became unavailable before we were able to complete all of the calculations in the planned series. Integration was performed in rectangular heliocentric coordinates.

It was assumed that  $\mu_1 = \mu_2$  in some series of calculations and that  $\mu_2 = 0.01\mu_1$  in others; here  $\mu_1$  and  $\mu_2$  are the ratios of the masses of the objects to the mass  $M_0$  of the central body. Initially circular orbits were considered in most series (Tables 1-9). With  $\mu_1 = 10^{-9}, 10^{-8}, 10^{-7}, 10^{-6}, 10^{-5}, 10^{-4}, 10^{-3}$  and  $\varphi_0 = 0, 60,$  and  $180^\circ$ , we investigated the ranges of  $\varepsilon_0 = (a_2^0 - a_1^0)/a_1^0$  that correspond to various types  $N_t$  of orbital-element variation (Tables 1-4), where  $\varphi_0$  is the initial angle at the central-body vertex between the lines to the objects (from the first object to the second) and  $a_1^0$  and  $a_2^0$  are the semimajor axes  $a$  of the initial orbits. The calculations dealt with the case  $a_2^0 > a_1^0$  because the nature and ranges of variation of the orbital elements when  $a_2^0 = a_1^0(1 - |\varepsilon_0|)$  are generally about the same as when  $a_2^0 = a_1^0(1 + |\varepsilon_0|)$ .

TABLE 2. Boundaries of  $\varepsilon_0$  Ranges Corresponding to Various Evolutionary Types  $N_t$  for  $e_1^0 = e_2^0 = 0$  and  $\varphi_0 = 60^\circ$

$\mu_1$	$10^{-3}$	$10^{-3}$	$10^{-7}$	$10^{-8}$	$10^{-9}$
$\mu_2$	$10^{-7}$	$10^{-7}$	$10^{-9}$	$10^{-10}$	$10^{-11}$
$T_0$	1000	25 000	25 000	25 000	25 000
$\delta_u$	0.285	0.293	0.0152	0.00855	0.00390
$\delta_r$	0.284	0.292	0.0151	0.0085	0.00389
$\beta_u$	0.0551	0.0532	0.00365	0.00174	0.000820
$\beta_L$	0.0550	0.0531	0.0036	0.00173	0.000815
$\alpha_u$	0.0535	—	0.00520	0.000165	0.0000519
$\alpha_e$	0.0533	—	0.00519	0.000164	0.0000518
$\alpha_r$	0.0533	—	0.00519	0.000164	0.0000518
$\mu_1$	$10^{-3}$	$10^{-3}$	$10^{-7}$	$10^{-8}$	$10^{-9}$
$\mu_2$	$10^{-7}$	$10^{-7}$	$10^{-9}$	$10^{-10}$	$10^{-11}$
$T_0$	1000	25 000	25 000	25 000	25 000
$\delta/\mu^{1/4}$	1.60	1.65	0.85	0.85	0.69
$\delta/\mu^{2/7}$	2.05	2.11	1.51	1.64	1.45
$\delta/\mu^{1/3}$	2.84	2.92	3.25	3.94	3.88
$\beta/\mu^{1/4}$	0.31	0.30	0.20	0.17	0.15
$\beta/\mu^{1/3}$	0.55	0.53	0.78	0.80	0.81
$\beta/h$	0.79	0.77	1.12	1.16	1.18
$\alpha/\mu^{1/3}$	0.53	—	0.11	0.076	0.052
$\alpha/\mu^{1/2}$	1.69	—	1.63	1.64	1.63
$T_0^2$	3.19	3.13	44.9	79.1	172
$N_3$	313	7990	557	316	145
$T_0^2$	12.9	13.4	185	385	816
$N_3$	77	1870	135	65	31

The case  $\varphi_0 = 60^\circ$  was investigated most thoroughly. The values of  $\varphi_0$  were varied in one of the series with  $\varepsilon_0 = 0$  (Table 7). We also determined the maximum orbital eccentricities that corresponded to the various types  $N_t$  and the periods of variation of the semimajor axes for objects that moved about triangular libration points (Table 9). In the series of calculations represented in Table 10,  $e_2^0 \neq 0$ ,  $\pi_1^0 = \pi_2^0 = 0$ ,  $\nu_1^0 = 0$ ,  $\nu_2^0 = 60^\circ$ , where  $e_k^0$ ,  $\pi_k^0$ , and  $\nu_k^0$  are the initial values of the eccentricity  $e$ , longitude of perihelion  $\pi$ , and the true anomaly  $\nu$  of the  $k$ -th object ( $k = 1, 2$ ).

The manner in which the variations of the elements  $e$ ,  $a/a_1^0$ , and  $\pi$  of the orbits vary with the number  $N_t$  of revolutions of the first object around the gravitating center is determined by the values of  $\mu_1$ ,  $\mu_2$ ,  $\varepsilon_0$ ,  $e_1^0$ ,  $e_2^0$ ,  $\pi_1^0$ ,  $\pi_2^0$ ,  $\nu_1^0$ , and  $\nu_2^0$ . These relationships are the same for all values of  $M_0$  and  $a_1^0$ . Only the time  $t_0 \propto (a_1^0)^{3/2} M_0^{-1/2}$  for one revolution around the central body will change when  $a \equiv a_1^0$ . The sun will be considered below as the central body. The covered time interval  $T_0$  ranged up to 25,000 revolutions of the first object around the sun.

### CALCULATIONS WITH INTEGRATION TO VARIOUS PRECISIONS ON A STEP

The BULSTO variable-step extrapolation of R. Bulirsh and J. Stoer [15] was used in integrating the equations of motion. In most of the variant calculations reported here (except for Figs. 1a, b, and d), integration on a step was accurate to  $\varepsilon_r = 10^{-8}$ . This value of  $\varepsilon_r$  was chosen [8] after comparison of orbital-element curves obtained with various  $\varepsilon_r$  and analysis of the variations of the energy and angular-momentum integrals during the calculations. In the course of evolution (at  $0 \leq N_t \leq T_0$ ), the energy and angular-momentum integrals varied least of all when  $\varepsilon_r \sim 10^{-8} - 10^{-7}$ , while the solutions obtained with  $\varepsilon_r = 10^{-8}$  and  $\varepsilon_r = 10^{-9}$  were closer to one another than those found with  $\varepsilon_r = 10^{-8}$  and  $\varepsilon_r = 10^{-7}$ . On the time intervals covered ( $T_0 \sim 10^4$ ), the time curves of the orbital elements were practically identical for  $\varepsilon_r = 10^{-8}$  and  $\varepsilon_r = 10^{-9}$  without close approaches of the MPs. It is therefore necessary to take  $\varepsilon_r \sim 10^{-9} - 10^{-8}$  for BULSTO calculations on a 48-place computer.

TABLE 3. Boundaries of  $\varepsilon_0$  Ranges Corresponding to Various Evolutionary Types  $N_t$  for  $e_1^0 = e_2^0 = 0$  and  $\varphi_0 = 60^\circ$

$\mu_1$	$10^{-3}$	$10^{-5}$	$10^{-5}$	$10^{-7}$	$10^{-7}$	$10^{-9}$	$10^{-9}$
$\mu_2$	$10^{-3}$	$10^{-5}$	$10^{-5}$	$10^{-7}$	$10^{-7}$	$10^{-9}$	$10^{-9}$
$T_0$	2500	2500	25 000	2500	25 000	2500	25 000
$\delta_0$	0,309	0,0725	0,0726	0,0182	0,0184	0,0045	0,00505
$\varepsilon_L$	0,308	0,0724	0,0725	0,0181	0,0183	0,00445	0,0050
$\gamma_H$	0,308	0,0651	0,0652	0,012	0,0140	0,00251	0,00305
$\gamma_L$	0,307	0,0650	0,0650	0,0115	0,0135	0,00250	0,00300
$\beta_H$	0,0646	0,0215	0,0210	0,00488	0,0046	0,00110	0,00102
$\beta_L$	0,0645	0,0214	0,0208	0,00487	0,00455	0,00109	0,00101
$\alpha_H$	—	0,00733	0,00733	0,000731	0,000731	0,0000731	0,0000731
$\alpha_L$	—	0,00732	0,00732	0,000730	0,00073	0,000073	0,000073
$\delta/\mu^{1/4}$	1,46	1,08	1,08	0,86	0,87	0,67	0,75
$\beta/\mu^{1/7}$	1,82	1,39	1,60	1,39	1,51	1,37	1,54
$S/\mu^{1/3}$	2,45	2,67	2,67	3,10	3,14	3,55	3,99
$\gamma/\mu^{1/3}$	2,44	2,40	2,40	2,01	2,35	1,99	2,40
$\gamma/h$	3,52	3,46	3,46	2,90	3,39	2,87	3,44
$\beta/\mu^{1/3}$	0,51	0,79	0,77	0,83	0,78	0,87	0,81
$\beta/h$	0,74	1,14	1,11	1,20	1,13	1,25	1,16
$\alpha/\mu^{1/3}$	—	0,27	0,27	0,12	0,12	0,058	0,058
$\alpha/\mu^{1/2}$	—	1,64	1,64	1,63	1,63	1,63	1,63
$\Delta C$	0,003	0,10	0,10	0,35	0,25	0,440	0,398
$\Delta A$	0,788	0,60	0,61	0,38	0,50	0,315	0,400
$\Delta M$	0	0,20	0,19	0,23	0,21	0,229	0,187
$\Delta N$	0,208	0,10	0,10	0,04	0,04	0,016	0,015

If the shortest distance between the MP objects is small, we can speak only of the statistical nature of the evolution and the ranges of variation of the orbital elements. In this case, curves of the orbital elements versus time that are obtained with various values of  $\varepsilon_r$  are for the most part similar only until the first very close encounter of the MPs. However, the nature and ranges of variation of the orbital elements are approximately the same.

We found on investigating the orbital evolution of two MPs that variation of  $\varepsilon_r$  had the strongest influence on the type of evolution in many cases when  $\mu_1 \geq 10^{-5}$ , and one of the MPs was ejected into a hyperbolic orbit in the course of evolution. When  $\mu_1 = \mu_2 = 10^{-5}$ , hyperbolic ejections were obtained only when the initial-orbit aphelion of the first MP was close to the initial-orbit perihelion of the second. Curves of  $a$ ,  $e$ , and  $\pi$  versus the number  $N_r$  of revolutions of the first MP around the sun are given in Fig. 1 for these cases. These variant calculations differ from one another in the values of  $\varepsilon_r$  and the initial values of  $\nu$ .

In the variants shown in Figs. 1a and c, one of the MPs was ejected into a hyperbolic orbit and the values of the orbital elements are given up to the close encounters that terminate in these ejections. In Fig. 1d, the time curves of  $a$  and  $e$  are presented without the two strong short-term heliocentric-orbit changes that occurred during very close approaches of the MPs. In the variant shown in this figure, the eccentricity of the osculating heliocentric orbit of one of the MPs reached large values ( $e \approx 1.7$  at  $N_r = 2200$  and  $e \approx 0.6$  at  $N_r \approx 4700$ ) during a brief period ( $\Delta N_r \leq 20$ ) and then returned to the neighborhood of the initial value. For real bodies (as against material points), collision rather than transfer of one of the bodies to a hyperbolic orbit may occur in some close encounters.

The results indicate that on variation of  $\varepsilon_r \in [10^{-11}, 10^{-7}]$ , the time curves of  $a$ ,  $e$ , and  $\pi$  change in about the same way as on variation of  $\nu_1^0$  and  $\nu_2^0$ . Although one of the MPs was ejected into a hyperbolic orbit in some of the cases, the maximum values of  $e$  and  $a$  in Fig. 1a-d are approximately the same for variant calculations:  $e_{\max} \approx 0.08-0.1$  and  $a_{\max} \approx 1.14-1.18$ . In the variants that appear in Figs. 1a-b, the objects entered the same 6:5 resonance and this ratio of their mean motions persisted for more than 100 revolutions.

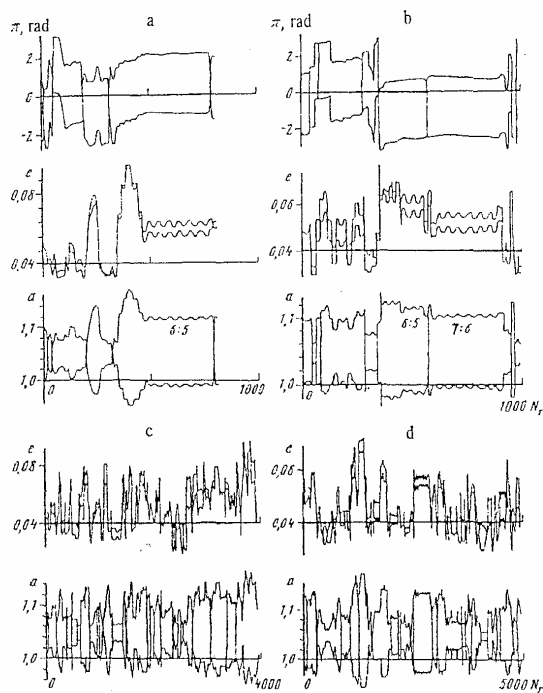


Fig. 1. Variations of semimajor axes  $a$  (for  $a_1^0 = 1$  a.u.), eccentricities  $e$  and perihelion longitudes  $\pi$  with time for two gravitationally interacting objects moving around the sun with close approaches to one another. The abscissa is the number of revolutions  $N_i$  of the first object around the sun. These results were obtained by numerical integration of the equations of motion of the plane three-body problem with various precisions  $\epsilon_i$  of integration on a step. Initial data:  $\epsilon_0 = 0.1$ ,  $\mu_1 = \mu_2 = 10^{-5}$ ,  $e_1^0 = e_2^0 = 0.05$ ,  $\pi_1^0 = 1$  rad,  $\pi_2^0 = 4$  rad. a)  $v_1^0 = 0$ ,  $v_2^0 = 2$  rad,  $\epsilon_i = 10^{-10}$ ; b)  $v_1^0 = 1$  rad,  $v_2^0 = 0$ ,  $\epsilon_i = 10^{-11}$ ; c)  $v_1^0 = 0$ ,  $v_2^0 = 2$  rad,  $\epsilon_i = 10^{-8}$ ; d)  $v_1^0 = 1$  rad,  $v_2^0 = 0$ ,  $\epsilon_i = 10^{-9}$ .

TABLE 4. Boundaries of  $\epsilon_0$  Ranges Corresponding to Various Evolutionary Types  $N_i$  for  $e_1^0 = e_2^0 = 0$  and  $T_0 = 2500$

$\mu_1$	$10^{-3}$	$10^{-3}$	$10^{-5}$	$10^{-5}$	$10^{-7}$	$10^{-7}$	$10^{-5}$	$10^{-5}$	$10^{-7}$	$10^{-7}$
$\mu_2$	$10^{-7}$	$10^{-7}$	$10^{-7}$	$10^{-7}$	$10^{-9}$	$10^{-9}$	$10^{-5}$	$10^{-5}$	$10^{-7}$	$10^{-7}$
$\psi_0$	0	180°	0	180°	0	180°	0	180°	0	180°
$\delta_4$	0.195	0.241	0.0461	0.0498	0.0141	0.0145	0.076	0.0722	0.0165	0.0176
$\delta_2$	0.194	0.240	0.0460	0.0497	0.0140	0.0144	0.0755	0.0721	0.0160	0.0175
$\beta_4$	—	0.0094	—	0.0160	—	0.00390	—	0.0202	—	0.0048
$\beta_2$	—	0.0093	—	0.0159	—	0.00389	—	0.0201	—	0.00475
$\delta/\mu^{1/4}$	1.09	1.35	0.82	0.88	0.79	0.81	1.13	1.08	0.77	0.83
$\delta/\mu^{2/7}$	1.40	1.73	1.23	1.33	1.40	1.44	1.67	1.59	1.33	1.44
$\delta/\mu^{1/5}$	1.94	2.40	2.13	2.30	3.02	3.10	2.79	2.66	2.74	3.00
$\beta/\mu^{1/3}$	—	0.094	—	0.74	—	0.84	—	0.74	—	0.82
$\delta/\delta_*$	0.67	0.825	0.84	0.91	0.93	0.96	1.05	0.996	0.895	0.967
$\beta/\beta_*$	—	0.17	—	0.93	—	0.99	—	0.939	—	0.979

TABLE 5. Examples of  $\epsilon_0$  Subranges Corresponding to Various Evolutionary Types  $N_i$  and Disposed Inside the Main Ranges for  $e_1^0 = e_2^0 = 0$  and  $\varphi_0 = 60^\circ$

$\mu_1$	$\mu_2$	$T_0$	Subranges of $\epsilon_0 = (a_2^0 - a_1^0)/a_1^0$
$10^{-3}$	$10^{-7}$	1000	0,0533W, 0,0534NM, 0,0535NM, 0,0538NMNM, 0,0539NMNM.
$10^{-3}$	$10^{-7}$	1000	0,0554NMA, 0,0541-0,0550M, 0,0551A,
$10^{-3}$	$10^{-7}$	2500	-0,233] {0,234} 0,235 h {0,236-0,252} {0,253-0,276} {0,277-
$10^{-9}$	$10^{-11}$	2500	-0,00137] {0,0014-0,00143} {0,00144-0,00185} {0,00186-
$10^{-5}$	$10^{-5}$	25 000	-0,065 ](0,0652-0,069) {0,07-0,0725} {0,0726-
$10^{-9}$	$10^{-9}$	2500	{0,00110-0,00226} {0,00227} {0,00228-0,00229}
$10^{-9}$	$10^{-9}$	2500	{0,0023-0,00242} {0,00243-0,0025} {0,00251-
$10^{-9}$	$10^{-9}$	25 000	-0,00225] {0,0023-0,0024} {0,00245-0,0025} {0,00255}
$10^{-9}$	$10^{-9}$	25 000	{0,0026 - 0,0030} {0,00305-

Note. The  $\epsilon_0$  ranges that correspond to the various types  $N_i$  appear in brackets: [type A], {type C}, (type P). A single bracket at the beginning (end) of a line corresponds to the upper (lower) limit of the range. The letter h indicates ejection of one of the objects into a hyperbolic orbit. The combination 0.0534NM in the first line of the table indicates that type N gave way to type M at  $\epsilon_0 = 0.0534$  after  $T_0 = 1000$  revolutions of the first object around the sun.

### Types of Orbital-Element Variation

Several types  $N_i$  of orbital-element variation can be distinguished for two gravitationally interacting objects [3-4, 7, 17, 20-21, 29-30, 38, 45]. In the case of initially circular orbits with  $24 \leq \varphi_0 \leq 336^\circ$ , these types are designated by the letters N, M, A, C, and P in order of increasing  $\epsilon_0 > 0$ .

Figure 2 shows curves of the semimajor axes  $a$ , eccentricities  $e$ , and perihelion longitudes  $\pi$  of the orbits plotted against the number of revolutions  $N_i$  of the first object around the sun. In most of these variant calculations,  $\mu_1 = \mu_2 = 10^{-7}$ . For initially circular orbits, the curves of  $e$  vs.  $N_i$  were practically identical for identical objects (Fig. 2a-e, g-h). Dozens of similar plots for other initial data will be found in the preprints [3-4].

For type N, the semimajor axes plot against time  $t$  in the form of N- or backward-N-shaped curves (Fig. 2a). Then the orbit of the second object in synodic coordinates (which revolve around the sun at the angular velocity of the first object) encloses one triangular libration point and takes the form of a tadpole (sickle) when  $e_1^0 = e_2^0 = 0$ . The origin of these coordinates is within the sun, one of the axes points toward the first object, and the second axis is perpendicular to the first.

TABLE 6. Values of  $\varphi_0$  that Correspond to the Boundary between Evolutionary Types A and M When  $a_2^0 = a_1^0$  and  $e_1^0 = e_2^0 = 0$  as Obtained by Solving Eq. (4) on the Basis of  $\beta_*$  Values

$\mu_1$	$10^{-3}$	$10^{-4}$	$10^{-5}$	$10^{-6}$	$10^{-7}$	$10^{-8}$	$10^{-9}$
$\beta_*$	0.531	0.75	0.79	0.8	0.78	0.8	0.81
$\varphi_0^*$	23,3°	9,51°	4,64°	2,25°	1,13°	0,51°	0,23°
$\varphi_0^*$ , rad	0.396	0.165	0.081	0.039	0.020	0.009	0.004
$\varphi_0^*/t^{1/2}$	4.07	3.58	3.76	3.92	4.25	4.11	4.04
$\varphi_0^*/t^{1/3}$	2.59	3.24	3.67	3.92	4.05	4.11	4.14

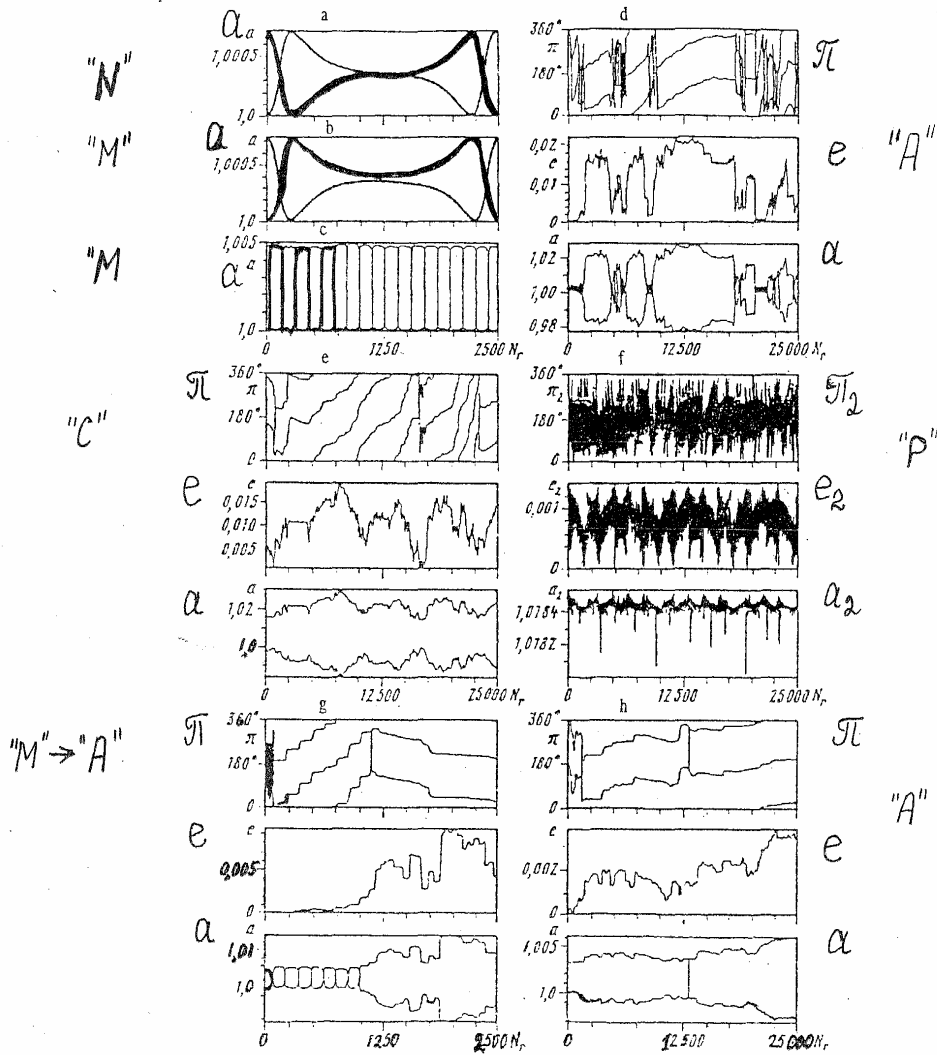


Fig. 2. Variations with time of semimajor axes  $a$  (for  $a_1^0 = 1$  a.u.), eccentricities  $e$ , and perihelion longitudes  $\pi$  of the orbits of two gravitationally interacting objects for various types  $N_t$ . The number of revolutions  $N_t$  of the first object around the sun is plotted against the axis of abscissas. Results obtained by numerical integration of the equations of motion of the plane three-body problem with  $\epsilon_r = 10^{-8}$ . In the variants shown in Figs. a-k,  $e_1^0 = e_2^0 = 0$ . In Figs. l-p,  $e_2^0 \neq 0$  and  $\pi_1^0 = \pi_2^0 = \nu_1^0 = 0, \nu_2^0 = 60^\circ$ : a)  $N_t = N, \mu_1 = \mu_2 = 10^{-7}, \epsilon_0 = 1.00073, \varphi_0 = 60^\circ$ ; b)  $N_t = M, \mu_1 = \mu_2 = 10^{-7}, \epsilon_0 = 1.000731, \varphi_0 = 60^\circ$ ; c)  $N_t = M, \mu_1 = \mu_2 = 10^{-7}, \epsilon_0 = 1.0048, \varphi_0 = 60^\circ$ ; d)  $N_t = A, \mu_1 = \mu_2 = 10^{-7}, \epsilon_0 = 1.0049, \varphi_0 = 60^\circ$ ; e)  $N_t = C, \mu_1 = \mu_2 = 10^{-7}, \epsilon_0 = 1.014, \varphi_0 = 60^\circ$ ; f)  $N_t = P, \mu_1 = \mu_2 = 10^{-7}, \epsilon_0 = 1.0184, \varphi_0 = 60^\circ$ ; g)  $N_t = M \Rightarrow A, \mu_1 = \mu_2 = 10^{-7}, \epsilon_0 = 1.0048, \varphi_0 = 180^\circ$ ; h)  $N_t = A, \mu_1 = \mu_2 = 10^{-9}, \epsilon_0 = 1.0030, \varphi_0 = 60^\circ$ ; j)  $N_t = P, \mu_1 = 10^{-3}, \mu_2 = 10^{-7}, \epsilon_0 = 1.295, \varphi_0 = 60^\circ$ ; k)  $N_t = P, \mu_1 = 10^{-3}, \mu_2 = 10^{-3}, \mu_3 = 10^{-7}, \epsilon_0 = 1, \varphi_0 = 60^\circ$ ; l)  $N_t = M, \mu_1 = \mu_2 = 10^{-7}, \epsilon_0 = 1.002, e_1^0 = 0, e_2^0 = 0.1$ ; m)  $N_t = A, \mu_1 = \mu_2 = 10^{-7}, \epsilon_0 = 1.07, e_1^0 = 0, e_2^0 = 0.1$ ; n)  $N_t = P, \mu_1 = \mu_2 = 10^{-7}, \epsilon_0 = 1.115, e_1^0 = 0, e_2^0 = 0.1$ ; o)  $N_t = M \Rightarrow A, \mu_1 = \mu_2 = 10^{-7}, \epsilon_0 = 1.005, e_1^0 = e_2^0 = 0.1$ ; p)  $N_t = A, \mu_1 = \mu_2 = 10^{-7}, \epsilon_0 = 1.01, e_1^0 = e_2^0 = 0.05$ .

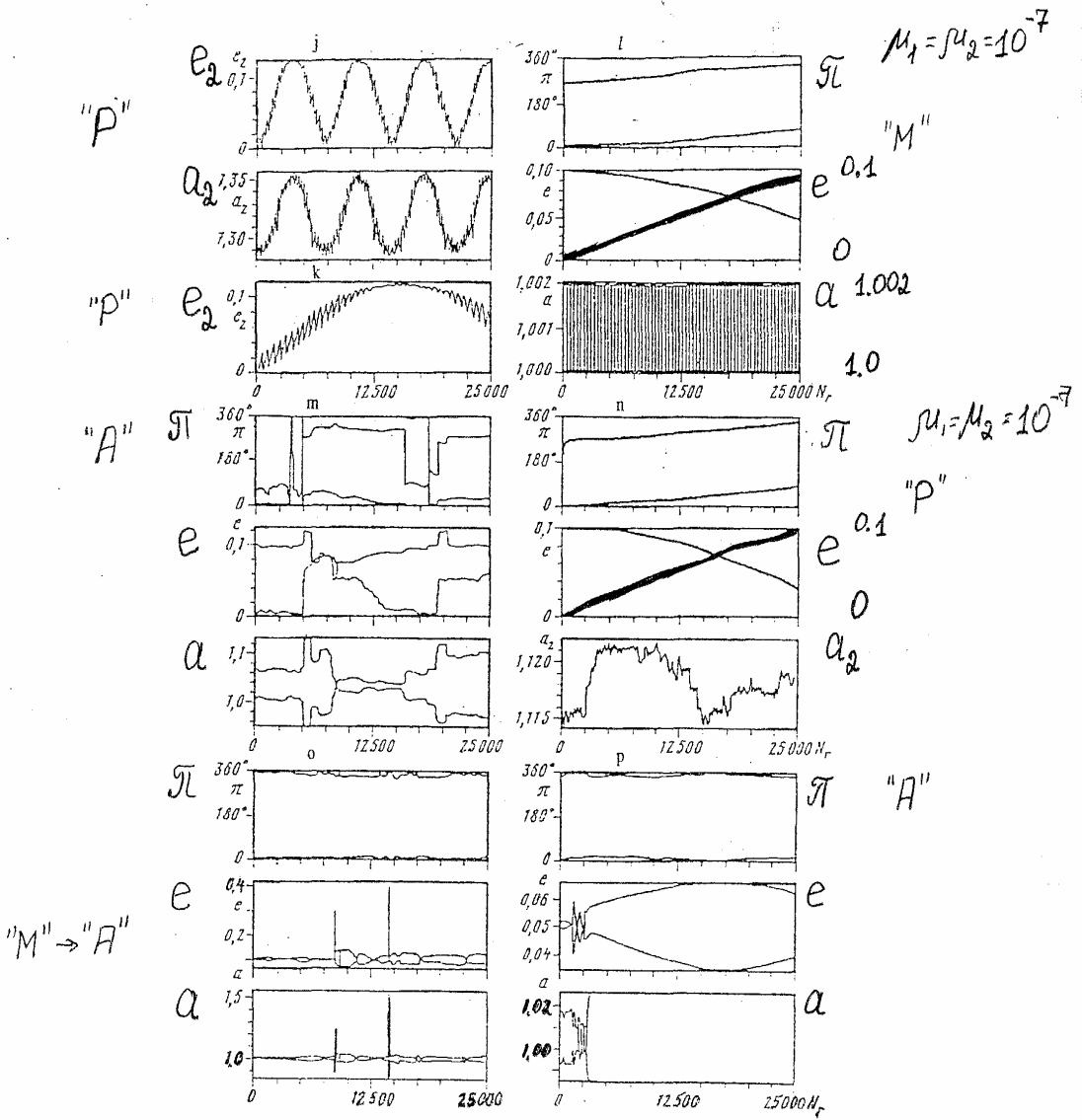


TABLE 7. Values of  $\varphi_0$  That Correspond to the Boundary between Evolutionary Types A and M When  $a_2^0 = a_1^0$  and  $e_1^0 = e_2^0 = 0$

$\mu_1$	$10^{-3}$	$10^{-5}$	$10^{-7}$	$10^{-9}$	$10^{-9}$	$10^{-3}$	$10^{-5}$	$10^{-7}$	$10^{-9}$	$10^{-9}$
$\mu_2$	$10^{-7}$	$10^{-7}$	$10^{-9}$	$10^{-11}$	$10^{-11}$	$10^{-3}$	$10^{-5}$	$10^{-7}$	$10^{-9}$	$10^{-9}$
$T_0$	2500	2500	2500	2500	25 000	2500	2500	2500	2500	25 000
$\varphi_{2a}$ , rad	0,451	0,087	0,0180	0,0035	0,0044	0,517	0,112	0,0231	0,046	0,0052
$\varphi_{1e}$ , rad	0,450	0,086	0,0179	0,0034	0,0043	0,516	0,111	0,0230	0,045	0,0051
$\varphi_B/M^2$	4,5	4,0	3,9	3,4	4,3	4,1	4,1	3,9	3,6	4,1
$\varphi_0/A$	6,5	5,8	5,6	5,0	6,3	5,9	5,9	5,7	5,2	5,9

TABLE 8. Periods of Orbital Semimajor-Axis Variations for Objects in Motion about Triangular Libration Points (with  $e_1^0 = e_2^0 = 0$ )

$\mu_1$	$\mu_2$	$T_M^*$	$T_M$	$T_M'$	$a_N$	$a_{St}$	$T_N^*$	$T_M^*$
$10^{-9}$	$10^{-9}$	1200	46 000	21 700	1,000073	1,0000731	2,1	4,4
$10^{-7}$	$10^{-7}$	270	5000	2200	1,000073	1,0060731	2,4	5,5
$10^{-5}$	$10^{-5}$	65	600	210	1,000732	1,000733	2,3	6,5
$10^{-9}$	$10^{-11}$	1600	63 000	32 300	1,0000518	1,0000519	2,5	4,8
$10^{-8}$	$10^{-10}$	670	17 700	9900	1,000164	1,000165	2,4	4,3
$10^{-7}$	$10^{-9}$	340	6600	3080	1,000519	1,000520	2,4	5,1
$10^{-6}$	$10^{-8}$	165	1630	870	1,00164	1,00165	2,1	4,0
$10^{-5}$	$10^{-7}$	80	600	300	1,00521	1,00522	2,3	4,7
$10^{-4}$	$10^{-6}$	40	180	80	1,0166	1,0167	1,9	4,3

TABLE 9. Maximum Eccentricities and Distances of Objects from the Sun for Various Evolutionary Types  $N_t$  When  $e_1^0 = e_2^0 = 0$

$N_t$	$\mu_1$	$10^{-3}$	$10^{-4}$	$10^{-5}$	$10^{-6}$	$10^{-7}$	$10^{-8}$	$10^{-9}$	$10^{-5}$	$10^{-7}$	$10^{-9}$
		$\mu_2$	$10^{-7}$	$10^{-6}$	$10^{-7}$	$10^{-8}$	$10^{-9}$	$10^{-10}$	$10^{-11}$	$10^{-5}$	$10^{-7}$
$P$	$e_{max}$	0,14	0,044	0,014	0,0065	0,0013	0,00056	0,00017	0,01	0,0014	0,0002
$C$	$e_{max}$	0,9	—	0,14	0,058	0,02	0,011	0,0041	0,09	0,019	0,0038
$C$	$e_H$	9	—	6,5	5,8	4,3	5,1	4,1	4,2	4,1	3,8
$C$	$e_h$	13	—	9,3	8,3	6,2	7,3	5,9	6,0	5,9	5,5
$C$	$R'_{max}$	>25	—	1,36	1,137	1,049	1,0246	1,01	1,26	1,05	1,01
$C$	$R'_{min}$	1,1	—	1,022	1,011	1,0034	1,0021	1,0009	1,045	1,009	1,0017
$C$	$\Delta R_\delta$	$\infty$	—	6,6	4,8	3,3	2,9	2,5	3,6	2,7	2
$C$	$\Delta R_\gamma$	0,43	—	0,42	0,48	0,34	0,46	0,48	0,7	0,65	0,55
$A$	$e_{max}$	1,0	0,32	0,16	0,08	0,038	0,013	0,007	0,10	0,027	0,0038
$A$	$e_H$	10	6,9	7,4	8	8	6	7	4,6	5,8	3,8
$A$	$e_h$	14	10	11	11,5	12	9	10	6,7	8,4	5,5
$A$	$R'_{max}$	$\infty$	1,9	1,305	1,15	1,07	1,029	1,0117	1,22	1,054	1,0076
$A$	$\Delta R_H$	$\infty$	19	14	15	15	13	12	8	9	6
$A$	$\Delta R_G$	$\infty$	9	5,6	5,3	4,6	3,4	3	3	3	1,5
$M$	$e_{max}$	0,04	0,01	0,006	0,0016	0,00056	0,00037	0,0007	0,003	0,0006	0,00013

Note.  $e_H = e_{max}/14^3$ ,  $e_h = e_{max}/h_1$ ,  $h_1 = (\mu_1/3)^{1/3}$ ,  $R'_{max} = R_{max}/a_1^0$ ,  $R'_{min} = R_{min}/a_1^0$ ,  $\Delta R_{HJ} = (R'_{max} - 1)/14^3$ ,  $\Delta R_\delta = (R'_{max} - 1)/\delta_*$ ,  $\Delta R_\gamma = (R'_{min} - 1)/\gamma_*$ .

In the case of type M, the  $a-t$  curves are M- or II-shaped (Figs. 2b-c, f, l). The orbit of the second object includes both triangular libration points in synodic coordinates. The synodic orbit is horseshoe-shaped when the sidereal orbits are initially circular. The distance from the sun to an object moving on an eccentric orbit varies from  $a(1 - e)$  to  $a(1 + e)$  as it revolves around the sun. Therefore the synodic orbits are of more complex form at higher  $e$  than in the case of initially circular sidereal orbits [4]. Even when  $e_1^0 = e_2^0 = 0$  in the case  $\mu_1 = \mu_2 = 10^{-3}$ , the horseshoe orbit in synodic coordinates crossed itself several times during the synodic period with an angle of about  $180^\circ$  between the lines to the objects [3].

Close approaches of the objects are possible only for type A (Fig. 2d, h, m). In this case the variations of the orbital elements are chaotic and the semimajor axes are identical at certain times.

When  $\mu_1 \geq 10^{-5}$  and  $N_t = A$ , the objects often entered resonant orbits in which their mean motions were commensurable for a certain time [3, 4]. Resonant orbits were obtained less often at smaller values of  $\mu_1$ , and the synodic periods were quite long. In the case shown in Fig. 2d, for example, the objects were in 19:18 resonance after  $16,000 \leq$

$N_1 \leq 17,500$ . There were almost no changes in  $e$  and  $\pi$ . We propose to discuss various cases in which the objects enter resonant orbits in greater detail in a separate paper.

For type C, the orbital elements vary chaotically, but there are no close approaches, and the semimajor axes cannot become identical (Fig. 2e).

If  $N_1 = P$ , then  $a$  and  $e$  vary periodically (Fig. 2f) and the synodic orbit of the second object encloses the sun as in the case of chaotic variations. Many subtypes can be distinguished within this type, each characterized by its own interrelationships between orbital-element variations. We discussed these interrelationships in [9] for the neighborhood of the 2:5 resonance with the motion of Jupiter. A. D. Bryuno [1] reviewed studies in which periodic orbits were considered within the framework of the plane circular restricted three-body problem.

In the case of initially circular orbits and  $\mu_1 = \mu_2$ , the difference  $\delta\pi = \pi_2 - \pi_1$  is generally about  $180^\circ$  during the evolution of all types  $N_1$ ; the values of  $\pi$  are more likely to increase (Figs. 2d, e, h), although they may also decrease (Fig. 2g).

### Ranges of Initial Data in Which the Orbital-Element Variations Are of the Various Types

Figure 3 shows a scheme of the  $\epsilon_0$  and  $\varphi_0$  ranges in which the orbital-element variations fall under the various types  $N_1$  in the case of initially circular orbits. As  $\epsilon_0$  increases when  $24 \leq \varphi_0 \leq 336^\circ$ , the ranges of types N, M, A, C, and P succeed one another in that order. The maximum values of  $\epsilon_0$  that correspond to ranges N, M, A, and C are denoted by  $\alpha$ ,  $\beta$ ,  $\gamma$ , and  $\delta$ . Since the boundary values of  $\epsilon_0$  are practically the same at  $\varphi_0$  and  $-\varphi_0$  (or  $360^\circ - \varphi_0$ ) and the range boundaries are about the same when  $\epsilon_0 = -|\epsilon_0|$  and  $\epsilon_0 = |\epsilon_0|$ , Fig. 3 represents the case  $0 \leq \varphi_0 \leq 180^\circ$  and  $\epsilon_0 \geq 0$ . The relationships among the values of  $\alpha$ ,  $\beta$ ,  $\gamma$ , and  $\delta$  that are presented in Fig. 3 were obtained with  $\mu_1 = 10^{-5} \gg \mu_2$ . Precise estimates of the boundary values of  $\epsilon_0$  were made only for  $\varphi_0 = 0, 60, \text{ and } 180^\circ$ , and approximate estimates were obtained for  $\varphi_0 = 120^\circ$ . As  $\mu_1$  decreases, there are more C orbits and fewer N and A orbits. The relative sizes of the  $\epsilon_0$  ranges that correspond to M, N, A, and C orbits are denoted by  $\Delta N = \alpha/\delta$ ,  $\Delta M = (\beta - \alpha)/\delta$ ,  $\Delta A = (\gamma - \beta)/\delta$ ,  $\Delta C = (\delta - \gamma)/\delta$  and are given in Tables 1 and 3.

Tables 1-4 give the ranges ( $\alpha_l, \alpha_u$ ), ( $\beta_l, \beta_u$ ), ( $\gamma_l, \gamma_u$ ), ( $\delta_l, \delta_u$ ) within which the values of  $\alpha$ ,  $\beta$ ,  $\gamma$ , and  $\delta$  fall for several values of  $\mu_1 \in [10^{-9}, 10^{-3}]$ ,  $\varphi_0$ , and  $T_0$ . These tables also give the ratios  $\alpha = (\alpha_l + \alpha_u)/2$ ,  $\beta = (\beta_l + \beta_u)/2$ ,  $\gamma = (\gamma_l + \gamma_u)/2$ , and  $\delta = (\delta_l + \delta_u)/2$  to  $\mu^{1/3}$ ,  $\mu^{2/7}$ ,  $\mu^{1/4}$ ,  $\mu^{1/2}$ , and  $h = (\mu/3)^{1/3}$ , where  $\mu = \mu_1 + \mu_2$  and  $h$  is the ratio of the radius of the Hill sphere to the distance  $R$  from the sun. The difference  $\alpha_u - \alpha_l$  represents the error with which  $\alpha$  is calculated. Since the period of the variations of  $a$  with time is much greater than  $T_0 = 2500$  when  $\mu_1 = 10^{-9}$  and  $N_1 = N$ , Table 1 gives no data in the  $\alpha$  column. In Table 2,  $T_\delta^s$  and  $T_\beta^s$  denote the synodic periods of revolution on fixed orbits with  $\epsilon_0 = 1 + \delta$  and  $\epsilon_0 = 1 + \beta$ , respectively;  $N_\delta = T_0/T_\delta^s$  and  $N_\beta = T_0/T_\beta^s$ .

Analytic estimates indicate [3] that the values of  $\alpha$  and  $\beta$  are largest when  $\varphi = \mp 60^\circ$ . In the series of calculations that we performed with  $\varphi_0 = 60^\circ$ , the values of  $\delta$  were generally larger than those for  $\varphi_0 = 0$  and  $\varphi_0 = 180^\circ$  (Table 4). We therefore focused on the case  $\varphi_0 = 60^\circ$ . The values of  $\alpha$ ,  $\beta$ ,  $\gamma$ , and  $\delta$  for  $\varphi_0 = 60^\circ$  are marked with asterisks:  $\alpha_*$ ,  $\beta_*$ ,  $\gamma_*$  and  $\delta_*$ .

The boundary values of  $\epsilon_0$  usually depend more strongly on  $\varphi_0$  for larger  $\mu_1$ . The dependence of  $\beta$  and  $\delta$  on  $\varphi_0$  is quite strong when  $\mu_0 = 10^{-3}$ . For example,  $\beta_*$  is more than five times larger than its value at  $\varphi_0 = 180^\circ$ . In the variants shown in Table 4,  $\delta/\delta_* \geq 0.84$  and  $\beta/\beta_* \geq 0.93$  when  $\mu_1 \leq 10^{-5}$ .

It follows from the results in Tables 1-3 that with  $\mu_1 \leq 10^{-4} \alpha_* = (1.63-1.64)\mu^{1/2}$ ,  $\beta_* = (0.77-0.81)\mu^{1/3}$ ,  $\delta_* = (2.1-2.45)\mu^{1/3}$ , and  $\gamma_* = (1.45-1.64)\mu^{2/7}$ . When  $\mu_1 = 10^{-3}$ , the values of  $\delta_*/\mu^{2/7}$  are larger ( $\approx 1.8 - 2.1$ ), those of  $\beta_*/\mu^{1/3}$  smaller ( $\approx 0.51-0.53$ ), and those of  $\gamma_*/\mu^{1/3}$  about the same ( $\approx 2.3-2.4$ ) as when  $\mu_1 \leq 10^{-4}$ .

Putting

$$\alpha_* = 1.6\mu^{1/2}, \beta_* = 0.8\mu^{1/3}, \gamma_* = 2.4\mu^{2/7}, \delta_* = 1.5\mu^{1/3}, \quad (1)$$

TABLE 10. Boundaries of  $\varepsilon_0$  Ranges Corresponding to Various Evolutionary Types  $N_i$  for  $\mu_1 = \mu_2 = 10^{-7}$ ,  $\pi_1^0 = \pi_2^0 = \nu_1^0 = 0$ ,  $\nu_2^0 = 60^\circ$  and  $T_0 = 25,000$

$\varepsilon_1^0$	0	0.0	0.1	$\varepsilon_1^0$	0	0.0	0.1
$\varepsilon_2^0$	0	0.1	0.1	$\varepsilon_2^0$	0	0.1	0.1
$\delta_4$	0.0184	0.12	0.015	$\beta_4$	0.00455	0.0020	0.0045
$\delta_2$	0.0183	0.115	0.01	$\alpha_4$	0.000731	0.00071	0.00071
$\beta_4$	0.0046	0.0025	0.005	$\alpha_1$	0.00073	0.0007	0.0007

$$\varepsilon_0 = \alpha_2^0 - \alpha_1^0$$

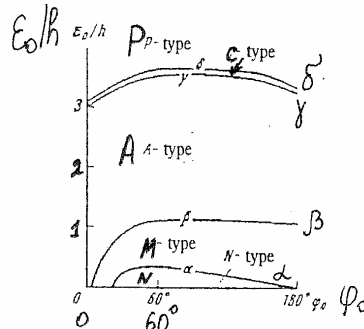
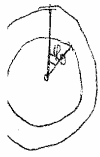


Fig. 3. Ranges of  $\varphi_0$  and  $\varepsilon_0/h$  (where  $h = (\mu/3)^{1/3}$ ) that correspond to various evolutionary types when  $\varepsilon_1^0 = \varepsilon_2^0 = 0$  and  $\mu_1 = 10^{-5} > \mu_2$ .

at  $\varphi_0 = 60^\circ$   
 $\delta_4 \approx 1.5 \mu^{2/7}$   
 $\gamma_4 \approx 2.4 \mu^{1/3}$   
 $\beta_4 \approx 0.8 \mu^{1/3}$   
 $\alpha_4 \approx 1.6 \mu^{1/2}$

we find that for  $\varphi_0 = 60^\circ$  the respective fractions of N, M, A, and C orbits are

$$\Delta N = \frac{\alpha}{\delta} = \frac{16}{15} \mu^{3/4}, \quad \Delta M = \frac{\beta - \alpha}{\delta} = \frac{8}{15} \mu^{1/2} |1 - 2\mu^{1/6}|, \quad (2)$$

$$\Delta A = \frac{\gamma - \beta}{\delta} = \frac{16}{15} \mu^{1/2}, \quad \Delta C = \frac{\delta - \gamma}{\delta} = 1 - 1.6 \mu^{1/2}.$$

The derivative of  $(\beta - \alpha)/\delta$  with respect to  $\mu$  is proportional to  $(\mu^{-20/21} - 9\mu^{-11/14})$  and positive when  $\mu < 9^{-6}$ . The ratio  $(\beta - \alpha)/\delta$  therefore decreases at these  $\mu$ , but it increases with decreasing  $\mu$  for  $\mu > 9^{-6}$ . The fraction of the earth to that of the sun. Since relations (1) are not satisfied exactly, the values of  $\Delta N$ ,  $\Delta M$ ,  $\Delta A$ , and  $\Delta C$  obtained from formulas (2) and in the calculations (Tables 1 and 3) may differ slightly. In the variant calculations considered,  $\Delta M \geq 0.19$  for  $\mu_1 \leq 10^{-5}$  and  $\varphi_0 = 60^\circ$ .

In some cases, N orbits became M orbits, P orbits became C orbits, and C and M orbits became A orbits as  $N_i$  increased. Examples of M-A transitions appear in Figs. 2g and 2o (they are keyed with the arrow  $\Rightarrow$  in the captions to these figures). In the case of  $N \Rightarrow M$ ,  $P \Rightarrow C$ ,  $C \Rightarrow A$ , and  $M \Rightarrow A$  transitions, the orbits are treated as types M, C, A, and A, respectively. At larger  $T_0$ , therefore, the values of  $\gamma$  and  $\delta$  may be larger and those of  $\beta$  smaller. At  $T_0 > 100T_s$  ( $T_s$  is the synodic period of revolution),  $\alpha$ ,  $\beta$ ,  $\gamma$ , and  $\delta$  depend only weakly on  $T_0$ . For example, in the case  $\mu_1 = 10^{-3}$  we have  $N_\delta = 313$  and  $N_\beta = 77$  at  $T_0 = 10^3$ , and the values of  $\delta$  and  $\beta$  differ by less than 4% from those obtained at  $T_0 = 2.5 \cdot 10^4$  (Table 2). Artymowicz [14] published curves of  $\gamma$  versus  $T_0$  for  $T_0 \leq 60T$ . In our series of calculations, the  $\beta$ ,  $\gamma$ , and  $\delta$  obtained for  $T_0 = 2500$  and  $T_0 = 25,000$  differed from one another by no more than 3, 17, and 22% - at  $\mu_1 \geq 10^{-5}$ ,  $\mu_1 \geq 10^{-7}$ , and  $\mu^{-9}$ , respectively.

When  $\mu_1 \leq 10^{-4}$ , we obtained no transitions between N and M orbits, i.e.,  $\alpha$  did not depend on  $T_0$ . When  $\mu_1 = 10^{-3}$ , N and M orbits might alternate with one another several times. The first two lines of Table 5 indicate the types  $N_i$  for several values of  $\varepsilon_0$ . For example, the combination 0.0538NMNM indicates that types N, M, N, and M followed one another in that order when  $\varepsilon_0 = 0.0538$  and  $T_0 = 1000$ . When  $\mu_1 = 10^{-3}$  and  $T_0 \geq 2500$ , M orbits always became A orbits. Therefore there are no values of  $\alpha$  in the corresponding columns of Tables 1 and 3, and  $\beta$  is the boundary between N and A orbits. When  $\mu_1 = \mu_2 = 10^{-3}$ ,  $T_0 = 2500$ , and  $\varphi_0 = 60^\circ$ , we have  $\beta \approx 0.065$ , but an M orbit persisted

through the first synodic period even when  $\varepsilon_0 = 0.11$ , i.e., the width of the  $\varepsilon_0$  range in which M orbits exist on a short time interval is comparable to  $\beta$ .

The letters  $\alpha$ ,  $\beta$ ,  $\gamma$ , and  $\delta$  are to be understood as the largest values of  $\varepsilon_0$  at which N, M, C, and A orbits, respectively, were obtained (at given  $\varphi_0$ ,  $\mu_1$ , and  $\mu_2$ ). In some cases, C orbits were obtained at certain values of  $\varepsilon_0$  in subranges of  $[\beta, \gamma]$ , and we have P orbits at certain  $\varepsilon_0 \in [\gamma, \delta]$ . Table 5 gives examples of such  $\varepsilon_0$  subranges. Let us discuss one of them. In the case  $T_0 = 25\,000$  and  $\varphi_0 = 60^\circ$ , the values of  $\varepsilon_0$  that correspond to the C-orbit subband lie in the range  $[0.75\gamma - 0.8\gamma]$  when  $\mu_1 = \mu_2 = 10^{-9}$ , while the boundaries of the P-orbit subband are  $0.9\delta$  and  $0.96\delta$  when  $\mu_1 = \mu_2 = 10^{-5}$ . The ratios  $\varepsilon_0/\mu^{1/3}$  for these two subbands lie in the respective intervals  $[1.8-1.9]$  and  $[2.4-2.56]$ .

### Comparison with Results of Other Authors

Let us compare the values that we obtained for  $\alpha$ ,  $\beta$ ,  $\gamma$ , and  $\delta$  with earlier results from other authors. In the plane circular restricted three-body problem, J. Wisdom [47] predicted theoretically that  $\delta = 1.3\mu^{2/7}$ , while M. Duncan et al. [20] used a mapping technique to find  $\delta = 1.49\mu^{2/7}$ . In our calculations, the values of  $\delta/\mu^{2/7}$  varied with  $\mu_1$  and  $\varphi_0$ , but averaged about 1.49 not only for  $\mu_1 > \mu_2$ , but also when  $\mu_1 = \mu_2$ . It was assumed in [3, 7, 19] that  $\delta \approx \mu^{1/4}$ . The values of  $\delta/\mu^{1/4}$  given in Tables 1-3 are close to unity at  $\mu_1 = 10^{-4}$  and  $\mu_1 = 10^{-5}$ . This ratio is lower for smaller  $\mu_1$ , but exceeds 0.69 when  $T_0 = 25,000$  and  $\mu_1 \geq 10^{-9}$ .

Investigating the Jacobi integral in the restricted three-body problem, J. Birn [16] showed that  $\gamma = \sqrt{12(\mu/3)^{1/3}} \approx 2.4\mu^{1/3}$ . Numerical calculations yielded  $\gamma = 2.1\mu^{1/3}$  for  $\varphi_0 = 0$  [22] and  $\gamma = 2.4\mu^{1/3}$  for  $\varphi_0 = 180^\circ$  [21]. With  $T_0 = 25,000$ , the values that we found for  $\gamma/\mu^{1/3}$  also averaged about 2.4 (Table 3). They could be smaller at smaller values of  $T_0$ .

The analytic estimate of  $\beta$  obtained in [28] was  $\sqrt{3.2h} \approx 1.24\mu^{1/3}$ . The numerical estimates of  $\beta$  given in the same study are even higher:  $1.9h \approx 1.3\mu^{1/3}$ . It was found in [38] that at the first conjunction all objects with  $1.75 \leq \varepsilon_0/h \leq 2.50$  enter the Hill sphere, and that when a longer time interval is considered,  $\beta = 1.5h \approx 1.04\mu^{1/3}$  and  $\gamma = 3h$ . The planetesimal A orbits for which  $\varepsilon_0 \leq 2.3h \approx 1.6\mu^{1/3}$  cross the orbit of the planet after times  $t < T_s$  [25]. The numerical studies of Kary and Lissauer [32] showed that most planetesimals approach to within 0.1h of the planet after  $20T_s$  when  $e = i = 0.9$  and  $0.9\mu^{1/3} < |\varepsilon_0| < 2.2\mu^{1/3}$ . We considered longer time intervals in our estimates. Therefore the values of  $\beta$  in Tables 1-4 are smaller than  $0.9\mu^{1/3}$ . B. Gladman [21] investigated the values of  $\gamma$  at  $\mu_1 = \mu_2$ . Other authors dealt for the most part only with the case  $\mu_1 > \mu_2$ .

The bands of  $\varepsilon_0$  values at which the objects collide after  $t < T_s$  has been investigated by several authors who studied the origin of axial rotation and the accretion rates of planets [26, 28, 33, 39, 43].

### Motion Near Triangular Libration Points

The motion of objects near triangular libration points has been discussed in [3, 7, 12, 17-18, 23, 34-35, 40-42, 45, 48]. Specific solar system bodies were usually chosen as the larger objects. It was shown analytically in [17] that  $\alpha \propto \mu^{1/2}$ .

In the plane restricted circular three-body problem, we found analytically in [3] that for N and M orbits

$$\varepsilon^2 \approx \varepsilon_s^2 - \frac{8}{3} \mu M(\varphi), \quad (3)$$

where  $M(\varphi) = (1 - \cos \varphi) + [2(1 - \cos \varphi)]^{-1/2} - 1.5$ ,  $\varepsilon_s$  is the value of  $\varepsilon = (a - a_1^\circ)/a_1^\circ$  and  $\varphi_0 = 60^\circ$ , and  $\varphi$  is the angle at the sun vertex between the lines to the second and first objects. It was assumed in deriving formula (3) that the orbits of the objects are nearly circular during evolution and that the values of  $\varphi$  are not very small. We note that  $M(\varphi) \geq 0$  for  $0 < \varphi \leq 180^\circ$ ,  $M(60^\circ) = 0$ ,  $M(180^\circ) = 1$ . Curves of  $M$  vs  $\varphi$  were given in [3]. Relation (3) describes the path of the object's relative motion in a rotating coordinate system one of whose axes is the line from the gravitating center to the first object.

Among other things, it follows from analysis of (3) that  $\alpha$  is largest when  $\varphi = 60^\circ$  and equal to  $\sqrt{8\mu/3} \approx 1.633\sqrt{\mu}$ . This value of  $\alpha$  agrees closely with the numerically calculated results in Tables 1-3. For type N orbits with  $\varepsilon =$

0, relation (3) can be used to determine the relation between the smallest and largest values of  $\varphi$  in the course of evolution:  $M(\varphi_{\min}) = M(\varphi_{\max})$  and  $0 < \varphi_{\min} < 60^\circ < \varphi_{\max} < 180^\circ$ .

The value of  $\varphi$  that corresponds to the boundary between N and M orbits when  $\varepsilon = 0$  is determined from the condition  $M(\varphi) = 1$  and  $0 < \varphi < 60^\circ$ . Let us denote this value by  $\varphi_\alpha$ . Substituting  $x = [1 - \cos \varphi]^{1/2}$  into relation (3), we obtain the cubic equation  $x^3 - 2.5x + 1/\sqrt{2} = 0$ . Solving it, we have  $\varphi_\alpha \approx 23.91^\circ$ .

Let  $\varphi_\beta$  be the value of  $\varphi$  that corresponds to the boundary between M and A orbits for  $\varepsilon = 0$ . If  $\beta_*$  is known,  $\varphi_\beta$  can be determined from the condition  $\beta_*^2 = (8/3)\mu M(\varphi_\beta)$  and  $0 < \varphi_\beta < 60^\circ$ , where  $\beta_*$  is the value of  $\beta$  for  $\varphi_0 = 60^\circ$ . Solving the corresponding cubic equation

$$x^3 - [1.5 + 3(\beta_*)^2/8\mu]x + 1/\sqrt{2} = 0, \quad (4)$$

we find  $\varphi_\beta$ . Table 6 gives values of  $\varphi_\beta^*/\mu^{1/3}$  and  $\varphi_\beta^c/\mu^{1/3}$ , where  $\varphi_\beta^*$  is the value of  $\varphi_\beta$  that solves (4) for the value of  $\beta_*$  given in the first line of this table, which is taken from Tables 1-2;  $\varphi_\beta^c$  is the value of  $\varphi$  obtained with  $\beta_* = 0.8\mu^{1/3}$ .

Table 7 gives the values  $\varphi_{\beta l}$  and  $\varphi_{\beta u}$  at the boundaries of the interval containing  $\varphi_\beta$ . These values were obtained by numerical integration of the three-body problem on time interval  $T_0$  for  $\varepsilon_0 = 0$  (i.e., for  $a_2^0 = a_1^0$ ). The values of  $\varphi_0$  in this series of calculations were varied so as to determine the interval  $(\varphi_{\beta l}, \varphi_{\beta u})$ . It was assumed in calculating  $\varphi_\beta/\mu^{1/3}$  and  $\varphi_\beta/h$  that  $\varphi_\beta = (\varphi_{\beta u} + \varphi_{\beta l})/2$ .

If the values of  $\varphi_\beta$  are taken in radians, the values of  $\varphi_\beta/\mu^{1/3}$  given in Table 7 lie for the most part in the range 3.9-4.3. With  $\mu_1 = 10^{-9}$ , increasing  $T_0$  from 2500 to 25,000 increases  $\varphi_\beta$  by about one-quarter. The values of  $\varphi_\beta^*/\mu^{1/3}$  in Table 6 are also close to 4. Only the values of  $\varphi_\beta^*/\mu^{1/3}$  for  $\mu_1 \geq 10^{-4}$  depart from 4 (ranging from 2.6 to 3.2), since in that case  $\beta_*/\mu^{1/3} \leq 0.75$ .

Putting  $1 - \cos \varphi_\beta \approx \varphi_\beta^2/2$  ( $\varphi_\beta$  in radians) and  $\varphi_\beta^2 \ll 2/\varphi_\beta$  in (3), we obtain  $\varphi_\beta = 2/3[1 + \beta^2/4\mu]^{-1}$ . If  $\beta = 0.8\mu^{1/3}$ , we have  $\varphi_\beta = 4\mu^{1/3}[1.5(0.64 + 4\mu^{1/3})]^{-1}$  with  $[1.5(0.64 + 4\mu^{1/3})]^{-1} \approx 1.04$  at  $\mu \approx 0$ .

According to [23], the smallest angle at the sun vertex between the lines to objects moving on horseshoe synodic orbits is  $\varphi^* = (8/3)\mu(1 + \varepsilon_0)^3/\varepsilon_0^2$ . Putting  $\varepsilon_0 = 0.8\mu^{1/3}$ , we find  $\varphi^*/\mu^{1/3} \approx 4.2$ . This value agrees with the results given in Tables 6-7.

For M-type orbits and  $60 \leq \varphi \leq 270^\circ$ , the smallest value of  $\varepsilon$  is obtained at  $\varphi = 180^\circ$ . Let us denote this value by  $\varepsilon_m$ . We see from Figs. 2b and 2c that  $\varepsilon_m$  is near zero when  $\varepsilon_0 \approx \alpha$  and  $\varepsilon_m \approx \varepsilon_* \approx \beta$  when  $\varepsilon_0 \approx \beta$ . Using relation (3) with  $\Delta\varepsilon = \varepsilon_* - \varepsilon_m \approx \varepsilon_*$ , we obtain  $\Delta\varepsilon \cdot \varepsilon_* = 4\mu/3$ . In that case,  $\Delta\varepsilon/\varepsilon_* \approx 1.33\mu/\varepsilon_*^2$ , and when  $\varepsilon_* = 0.8\mu^{1/3}$  we have  $\Delta\varepsilon/\varepsilon_* \approx 2.08\mu^{1/3}$ . It is seen from this formula that the M-shaped variations of  $a$  become more II-shaped for smaller  $\mu$ . As a result,  $\beta$  is almost independent of  $\varphi_0$  at small  $\mu_1$ .

Table 8 gives the calculated periods  $T_M$  and  $T'_M$  of horseshoe synodic orbital motions for  $\varepsilon_0 \approx \alpha$  and  $\varepsilon_0 \approx \beta$ , respectively.  $T_N$  is the longest period of the motion on a tadpole synodic orbit when  $\varepsilon_0 \approx \alpha$ . The unit of time is the period of revolution of the first object around the central body. The values of  $a^0/a_1^0$  that correspond to the periods  $T_N$  and  $T_M$  when  $\varphi_0 = 60^\circ$  are denoted by  $a_N$  and  $a_M$ ;  $T^s_N = T_N/T'_s$  and  $T^s_M = T_M/T'_s$ , where  $T'_s$  is the synodic period of revolution for motion of the objects on fixed initial orbits. It is seen from Table 8 that  $T^s_N$  is usually greater than two, while  $T^s_M \sim 4-6$ . The smaller the  $\mu_1$ , the larger is the ratio  $T_M/T'_M$ ; it approaches 40 when  $\mu_1 = 10^{-9}$ .

When  $\varepsilon_0 \approx \beta$ ,  $\varepsilon \approx \varepsilon_0$  for most of the time, while the angle  $\varphi$  changes by about 2 (6.28 -  $8\mu^{1/3}$ ) radians during the period  $T'_M$ . As a result, the values of  $T'_M$  given in Table 8 for  $\mu_1 \leq 10^{-4}$  are only slightly smaller than  $2T'_s$  and larger than  $1.9T'_s$ .

As  $|\varepsilon_0 - \alpha|$  becomes smaller, the period of the motion on the synodic orbit becomes longer for  $N_i = N$  and shorter for  $N_i = M$ . The data in Table 8 are given for  $\varphi_0 = 60^\circ$ . Larger values of  $T^s_M$  are obtained for the cases  $\varepsilon_0 = \alpha$  and  $\varphi_0 = 180^\circ$ . For example,  $T^s_M = 14$  when  $\mu_1 = \mu_2 = 10^{-5}$ .

Periods  $T_l$  were given in [45] for several synodic orbits near the triangular libration points of the sun-earth system. Dermott [18] considered the periods of motion on type N orbits and gave a relation for  $T_l$  as a function of  $\varphi_{\max}$  for  $\varphi_{\max} \leq 165^\circ$ , where  $\varphi_{\max}$  is the maximum value of  $\varphi$  during evolution. For  $\varphi_{\max} \approx 60^\circ$ , the result was  $T_l = 2/(2.7\mu)^{1/2}$ , where the period of revolution of the first object around the sun is taken as the unit of time.

## Maximum Eccentricities and Distances from Sun

To estimate the interactions of a large number of planetesimals on the basis of their pairwise interactions it is necessary to know the maximum values of the eccentricities  $e_{\max}$  and distances  $R_{\max}$  obtained for the planetesimals from study of the three-body problem over time  $T_0$ . These values are given in Table 9 for the various types  $N_t$ . Types  $N_t = A$  and  $N_t = C$  are of the greatest interest for cosmogonic problems. Since the variations of  $a$  and  $e$  are small for  $N_t = N$ , no data are given. In the present section, as above, we shall consider the case of initially circular orbits.

In the case  $\mu_1 \leq 10^{-5}$ , the values of  $e_H = e_{\max}/\mu_1^{1/3}$  do not usually exceed 7-8 for  $\mu_1 \gg \mu_2$  or 4-6 for  $\mu_1 = \mu_2$  for type A and 4-6 for  $\mu_1 \gg \mu_2$  and 4 for  $\mu_1 = \mu_2$  for type C. For  $N_t = C$ , the values of  $e_H$  are for the most part slightly smaller for smaller  $\mu_1$ . For comparison with several other studies, Table 9 gives values of  $e_h = e_{\max}/h_1$ , where  $h_1 = (\mu_1/3)^{1/3}$ . References [26-27, 38-39] give values of the  $e_h$  acquired by a particle in a close approach to the planet. The largest values,  $e_h \approx 5$ , were obtained for a very small fraction of the  $e_0$  values. They are half as large as the  $e_h$  that we obtained at  $T_0 = 25,000$ .

Table 9 also gives the maximum (among the variants studied) values  $R'_{\max} = R_{\max}/a_1^0$ ,  $\Delta R_H = (R'_{\max} - 1)/\mu_1^{1/3}$  and  $\Delta R_\delta = (R'_{\max} - 1)/\delta_*$  and the minima  $R'_{\min} = R_{\min}/a_1^0$  and  $\Delta R_\gamma = (R'_{\min} - 1)/\gamma_*$ , where  $R_{\max}$  and  $R_{\min}$  are the largest and smallest values, respectively, of the distance  $R$  between the second object and the gravitating center in the course of evolution. The values of  $\Delta R_\delta$  are larger for larger  $\mu_1$  and for objects of unequal mass. In the case of type A, the values of  $\Delta R_\delta$  are 1.5 when  $\mu_1 = \mu_2 = 10^{-9}$  and 5.6 when  $\mu_1 = 10^{-5} \gg \mu_2$ . They are slightly larger for type C at 2 and 6.6, respectively. For type C and  $\mu_1 \gg \mu_2$ , the values of  $\Delta R_\gamma$  always exceeded 0.4. Since  $\gamma_* \geq 3h$ , the distance between the objects when  $N_t = C$  was always greater than the radius of the corresponding Hill sphere.

When  $\mu_1 = 10^{-3}$ ,  $a$ ,  $R$ , and  $e$  vary widely with time, and the second object may retreat to any distance from the central body. Therefore  $R'_{\max}$ ,  $\Delta R_\delta$ , and  $\Delta R_H$  are represented by  $\infty$  in the corresponding column of Table 9. In several cases with very close approaches of the objects, the osculating eccentricities may be several times the  $e_{\max}$  values in Table 9. When the objects emerge from the Hill sphere, the values of  $e$  generally decrease (see also Sec. 13 of [10]). Figure 20 gives examples of these eccentricity and semimajor-axis jumps for a case of initially eccentric orbits. Similar plots for initially circular orbits will be found in [3].

The ranges  $\Delta e$  of  $e$  for type A are more than twice  $e_{\max}$ . The ratio  $\Delta e/e_{\max}$  may exceed 10 for types N and M. When  $N_t = P$ , on the other hand,  $\Delta e < e_{\max}$ .

For  $T_0 = 25,000$  and  $\mu_1 = \mu_2$ , the ratios  $(\delta_* - \gamma_*)/(\gamma_* - \beta_*)$  of the fractions of C and A orbits with  $\mu_1 = 10^{-5}$ ,  $\mu_1 = 10^{-7}$ , and  $\mu_1 = 10^{-9}$  are 0.17, 0.5, and 1, respectively. For  $T_0 = 2500$  and  $\mu_2 = 0.01\mu_1$ , these ratios were found to be 0.05, 0.063, and 2.4 for the  $\mu_1$  values given above. For type C, the difference  $R - a_1^0$  may be several times larger at the end of evolution. It is therefore necessary to consider the interaction of the bodies not only when  $e_0 < \gamma$ , but also for  $\gamma \leq e_0 \leq \delta$  in a disk that consists of a large number of small planetesimals moving on almost circular orbits.

In the case of initially circular orbits, the orbits of the  $\mu_2$  objects for which  $e_0 < \delta$  may change significantly under the influence of a  $\mu_1$  planetesimal (collisions occurring only if  $e_0 < \gamma < \delta$ ). These objects may collide with planetesimals whose semimajor axes differ from  $a_2^0$  by  $\Delta R_\delta a_2^0$ . Therefore if the difference between the semimajor axes of the orbits of neighboring planetesimals in the disk is smaller than  $\Delta R_\delta a$ , their effects on smaller objects must be considered jointly.

Let  $N$  identical bodies with a total mass  $\eta m_\oplus$  move on orbits whose semimajor axes  $a_k = a_p(1 - d + 2dk/N)$ , where  $m_\oplus$  is the mass of the earth,  $2da_p$  is the width of the swarm of bodies, and  $k$  is the number assigned to the body. In this case,  $\gamma \approx 2.4(2\eta\mu_\oplus/N)^{1/3}$  and  $\delta \approx 1.5(2\eta\mu_\oplus/N)^{2/7}$  for any pair of bodies, where  $\mu_\oplus$  is the ratio of the mass of the earth to the mass of the sun. Let us denote the semimajor axis of the orbit of one of the bodies by  $a_*$ . The average number of bodies for which  $Da = |a_k - a_*| \leq \gamma$  and  $Da \leq \delta$  is approximately  $N_\gamma = 2\gamma/(2d/N) = 2,4(2\eta\mu_\oplus)^{1/3}N^{2/3}/d \approx 0,044N^{2/3}\eta^{1/3}/d$ ,  $N_\delta = 2\delta/(2d/N) = 1,5(2\eta\mu_\oplus)^{2/7}N^{5/7}/d \approx 0,048N^{5/7}\eta^{2/7}/d$ . Setting  $\eta = 1$  and  $d = 0.24$  for the zone of the earth, we obtain  $N_\delta > N_\gamma > 1$  if  $N > 13$ , with  $N_\gamma = 8.5 \cdot 10^3$  and  $N_\delta = 2 \cdot 10^4$  for  $N = 10^7$ . The values of  $\eta$ ,  $N_\gamma$ , and  $N_\delta$  are larger for the zones of the giant planets than for that of the earth. These approximate estimates indicate that if the masses of the planetesimals in the feeding zone of a planet do not differ greatly at a certain time, each planetesimal may closely approach a large number of neighboring planetesimals. This inference is also valid for a three-dimensional model owing to the variations of the perihelion and ascending-node longitudes of the planetesimals.

## The Case of Initially Eccentric Orbits

It has been found in studies of the circular three-body problem in the case  $\mu_2 \leq \mu_1 \ll 1$ ,  $e \ll 1$ ,  $i \ll 1$ , and  $a \approx \text{const}$  [14, 28, 31] that  $\gamma^2 = 4(e^2 + i^2)/3 + 12h^2$ . Therefore  $\gamma$  is larger the larger  $e$  and  $i$ . The calculations in [34] indicate that  $\beta$  decreases with increasing  $i$ . An increase of  $\gamma$  and a decrease of  $\beta$  with increasing  $e$  were also found in [26, 43] after a time  $T_0 < T_s$ .

In the series of calculations of  $E_1$  and  $E_2$  in Table 10, it was assumed that  $\mu_1 = \mu_2 = 10^{-7}$ ,  $T_0 = 25,000$ ,  $e_2^0 = 0.1$ ,  $\pi_1^0 = \pi_2^0 = 0$ ,  $\nu_1^0 = 0$ , and  $\nu_2^0 = 60^\circ$ , with  $e_1^0 = 0$  (series  $N_s = E_1$ ) or  $e_1^0 = 0.1$  ( $N_s = E_2$ ). This table gives the ranges of  $(\alpha_l, \alpha_u)$ ,  $(\beta_l, \beta_u)$ , and  $(\delta_l, \delta_u)$  in which the values of  $\alpha$ ,  $\beta$ , and  $\delta$  fall.

The results in Table 10 indicate that the values of  $\alpha$  for  $e_1^0 \neq 0$  are only slightly smaller than for initially circular orbits. When  $e_2^0 = e_1^0$ , the values of  $\beta$  are approximately the same as for  $e_2^0 = e_1^0 = 0$ , but are half as large when  $e_1^0 = 0$  and  $e_2^0 = 0.1$ . The values of  $\delta$  for  $e_2^0 = e_1^0 = 0.1$  are even smaller than those for initially circular orbits, but for  $e_1^0 = 0$  and  $e_2^0 = 0.1$  they are several times as large. For  $e_2^0 = \text{const}$ , therefore, the values of  $\beta$  and  $\delta$  may depend strongly on  $e_1^0$ . They also vary as functions of the initial orientations of the orbits of these objects and of the initial positions of the objects on the orbits. For  $N_s = E_2$ , the initial orbits of the objects are similar and identically oriented. Therefore close approaches of these objects occur in a narrow range of  $\varepsilon_0$ .

The orbital elements of the objects in the case  $e_2^0$  are plotted against time in Figs. 2l-2p. We published more than 20 other diagrams of this type in [4] (most of them for  $e_1^0 = e_2^0$ ).

In the case of type M, the variations of  $a$  for initially eccentric orbits are approximately the same as those for initially circular orbits. But when  $\varepsilon_0 = \max\{e_1^0, e_2^0\} \neq 0$ , the amplitude  $\Delta e_k = e_{\max}^k - e_{\min}^k$  ( $k = 1, 2$ ) of the long-period variations of  $e_k$  may exceed  $\varepsilon_0$  and may be hundreds of times the values of  $e_{\max}$  obtained with  $\varepsilon_0 = 0$  for the same object masses [4]. In the variant of the  $N_s = E_1$  series given in Fig. 2l ( $\varepsilon_0 = 0.002$ ), the eccentricity of the orbit of the first object increased from 0 to 0.09 during  $T_0 = 25,000$ . With the same values  $\mu_1 = \mu_2 = 10^{-7}$  in the case  $\varepsilon_0 = 0$ ,  $e_{\max} \leq 0.0006$  for type M, and we even found  $e_{\max} \leq 0.03$  for type A. The values of  $e_{\max}$  for  $N_t = M$  and  $N_t = N$  are smaller for smaller  $\varepsilon_0$ . For example, in the series  $N_s = E_1$  with  $0.0007 \leq \varepsilon_0 \leq 0.00073e_{\max} \approx 0.005$  is hardly more than 1/20 of the value when  $\varepsilon_0 = 0.002$ .

For  $N_s = E_2$  and  $N_t = M$ , the amplitude of the long-period variations of  $e$  is no more than twice that of the variations of  $e$  during the period  $T_a$  of the variations of  $a$  and  $\Delta e = \max\{\Delta e_1, \Delta e_2\} \leq 0.0012$ . The period  $T_e$  of the long-period variations is smaller for smaller  $\varepsilon_0$ . For example,  $T_e = 11,000$  for  $\varepsilon_0 = 0.003$  and  $T_e = 3500$  for  $\varepsilon_0 = 0.004$ . It was found for  $N_s = E_2$  and  $\varepsilon_0 = 0.0007$  that  $N_t = N$ , and that the amplitude of the long-period variations of  $e$  ( $T_e \gg T_0 = 25,000$ ) significantly exceeds the variations of  $e$  during the period of variation of  $a$ , so that the variations of  $e$  after  $T_0$  ( $\Delta e \approx 0.0015$ ) are larger than when  $N_t = N$ .

In the case  $N_t = N$  or  $N_t = M$ , we obtained  $\delta\pi = \pi_2 - \pi_1 \approx 90^\circ$  with  $N_s = E_1$  and  $\pi_2 \approx \pi_1 \approx 0$  for  $N_s = E_2$ . In the variant of the  $N_s = E_1$  series in Fig. 2l,  $\pi_1$  and  $\pi_2$  increased by about  $70^\circ$  during  $T_0 = 25,000$ .

In the variants with  $\mu_1 = 10^{-5}$  and  $N_t = M$ , the values of  $\pi_2$  (and  $\pi_1$  if  $\mu_1 = \mu_2$ ) increased by  $360^\circ$  during the period  $T_e$  ( $T_e \geq 2500$ ) of the long-period variations of  $e$ , and when  $\mu_1 \gg \mu_2$  the values of  $e_2$  reached their maximum at  $\delta\pi = 0$  and their minimum at  $\delta\pi = 180^\circ$  if  $e_1^0 = e_2^0$  and, conversely, peaked at  $\delta\pi = 180^\circ$  and bottomed at  $\delta\pi = 0$  if  $e_1^0 = 0$  and  $e_2^0 = 0.05$  [4]. When  $\mu_1 = \mu_2$ , the maximum of  $e_2$  corresponds to the minimum of  $e_1$ . The increase in  $\pi_2$  and the variation of  $e_2$  took place in small steps. The time after which a new step appeared was equal to half the period of variation of  $a_2$ , with the main changes in  $a$ ,  $e$ , and  $\pi$  occurring simultaneously.

The values of  $e_{\max}$  and  $\Delta e_k$  can depend strongly on the initial orientations of the orbits. In the case  $\mu_1 = \mu_2 = 10^{-5}$ ,  $\varepsilon_0 = 0.01$ ,  $e_1^0 = e_2^0 = 0.05$ ,  $\nu_1^0 = 1$  rad, for example, the values of  $\Delta e_k$  are several times larger for  $\delta\pi_0 = \pi_2^0 - \pi_1^0 = 3$  rad and  $\nu_2^0 = 2$  rad than for  $\delta\pi_0 = 2$  rad and  $\nu_2^0 = 0$  rad [4]. We note that  $\delta\pi \approx 180^\circ \approx \delta\pi_0$  at all times in the first of these variant calculations, and that  $\delta\pi$  varied with the period  $T_e$  in the second variant.

Studies of type M orbits indicate that clusters of planetesimals whose semimajor axes are the same as those of the forming planets may exist during the evolution of a protoplanetary disk.

When  $N_t = A$ , the values of  $\Delta e$  and  $e_{\max}$  are larger for larger  $e_1^0$  and  $e_2^0$  [4]. In many of the variant calculations, it was found that  $\Delta e > \varepsilon_0$  for large  $T_0$  (Figs. 2m and 2o). For a given  $\mu_1$ , the values of  $\Delta e$  were usually larger for  $\mu_1 \gg \mu_2$  than for  $\mu_1 = \mu_2$ . For  $\mu_1 = \mu_2$  and  $e_1^0 = e_2^0$ , the time curves of  $e_1$  and  $e_2$  were almost identical in some cases and almost symmetric about  $\varepsilon_0$  in others. Acquisitions of resonant orbits were found more frequently when the initial orbits

were eccentric than when  $e_1^0 = e_2^0 = 0$  [4].

In the variant in Fig. 2p, several close approaches were followed by a period of "stabilization" in which  $a$  remained almost constant for a long period of time while  $e$  varied periodically. The maximum of  $e_2$  and the minimum of  $e_1$  during this time were obtained with  $\delta\pi = 0$ , and the perihelion distances of the objects were similar.

For  $N_t = C$ , the ranges of  $e$  and  $a$  may be about the same as for  $N_t = A$ . Figure 2n represents a case in which the chaotic variations of  $a$  were comparatively minor and the  $e(t)$  curves were sinusoidal with  $\Delta e \approx 0.1$ .

In the case  $N_t = P$  with  $N_s = E_1$ , we obtained  $\pi_1 \approx 270^\circ$  and  $\pi_2 \approx 0$ , but when  $N_s = E_2$  the values of  $\pi$  hardly changed and the curves of  $e_1$  and  $e_2$  against time were "symmetric" about  $e_1^0 = e_2^0 = e_0$ . The periods of the long-period variations of  $e$  were longer for large  $e_0$ .

It was shown that  $a_2$  decreased from 1.7 to 1.1 during  $T_0 = 10^{-4}$  when  $\mu_1 = \mu_\oplus \gg \mu_2$ ,  $\varepsilon_0 = 0.7$ ,  $e_1^0 = 0$ ,  $e_2^0 = 0.5$ . This result indicates that the orbits of asteroids that cross the earth's orbit vary strongly over the characteristic time to collision with the earth ( $\sim 4 \cdot 10^{-7}$  yr) and that the lifetimes of these asteroids do not depend strongly on their initial orbits.

### Conclusion

The orbital evolution of about a thousand pairs of gravitationally interacting bodies – material points (MPs) in motion around the sun – was investigated by numerical integration of the plane three-body problem. We studied the characteristic variations of the orbits for the following orbital-evolution types: motion about triangular libration points on adpole and horseshoe synodic orbits (types N and M), the case of close approaches (to the radius of the sphere of influence) of A-type objects, and chaotic variations of the orbital elements in which close approaches of the MPs are not possible (type C). The ratio  $\mu_1$  of the mass of the larger MP to the mass of the sun was varied from  $10^{-9}$  to  $10^{-3}$ , and we considered not only the restricted three-body problem, but also the case of identical MPs ( $\mu_1 = \mu_2$ ). The time interval considered in most of the series of calculations was 2500 or 25,000 revolutions of the objects around the sun.

With time, certain N orbits may become M orbits, and C and M orbits may become A orbits. Such transitions are rare when  $t > 100T_s$  ( $T_s$  is the synodic period of revolution). In the case of initially circular orbits ( $e_0 = 0$ ), an initial angle  $\varphi_0 = 60^\circ$  between the lines to the objects at the sun vertex,  $10^{-9} \leq \mu_1 \leq 10^{-4}$ , and a time interval  $T_0 \sim 10^4 t_0$  ( $t_0$  the time in which the first MP revolves around the sun), the maximum values of  $e_0 = (a_2^0 - a_1^0)/a_1^0$  for  $N_t = N, M, C$  were found to be  $\alpha = (1.63-1.64) \cdot \mu^{1/2}$ ,  $\beta = (0.77-0.81) \cdot \mu^{1/3}$ ,  $\gamma = (2.1-2.45) \cdot \mu^{1/3}$  and  $\delta = (1.45-1.64) \cdot \mu^{2/7}$ , respectively. The values of  $\alpha$ ,  $\beta$ , and  $\delta$  were generally smaller for other values of  $\varphi_0$ . The case  $\varphi_0 = 60^\circ$  had not been considered previously, and the values of  $\beta$  could not be estimated accurately. When  $\mu_1 = 10^{-3}$ , type M orbits are stable; for  $\varphi_0 = 60^\circ$  we found  $\alpha = \beta \approx 0.5\mu^{1/3}$ ,  $\gamma = (1.8-2.1) \cdot \mu^{1/3}$  and  $\delta = (2.3-2.4) \cdot 10^{2/7}$ , and for other  $\varphi_0$  the values of  $\delta$  and  $\beta$  could be smaller by one-third and by factors larger than 5, respectively. When  $\mu_1 \leq 10^{-5}$ , the values of these quantities generally differed by no more than 10% as  $\varphi_0$  was varied. Each planetesimal in a protoplanetary disk could make close approaches to several of its neighbors.

When  $10^{-9} \leq \mu_1 \leq 10^{-4}$  and  $\varphi_0 = 60^\circ$ , the fraction of M orbits, i.e., the ratio  $(\beta - \alpha)/\delta$ , varied in the range 0.18–0.25. As  $\mu_1$  was reduced, the fractions of N and A orbits declined and the fraction of C orbits increased. The fractions of C and A orbits were about equal ( $\gamma - \beta \approx \delta - \gamma$ ) when  $\mu_1 = \mu_2 = 10^{-9}$ .

C orbits were obtained in some cases at certain  $\varepsilon_0$  in a subrange of  $[\beta, \gamma]$ , and the orbital elements varied periodically at certain  $\varepsilon_0 \in [\gamma, \delta]$ .

Motion near triangular libration points was investigated analytically as well as numerically. With  $e_0 = 0$ , it was found that the maximum values of  $\varphi_0$  that correspond to N and M types were close to  $0.4$  and  $4\mu^{1/3}$  rad. The curves  $a$  plotted against time are N- or M-shaped. The smaller  $\mu$ , the more strongly did the M-shaped  $a$  curves resemble  $\Pi$ -shaped curves. The periods of the variations of  $a(t)$  were longest for N and M orbits when  $\varepsilon_0 \approx \alpha$  and could be as long as 2–6 times larger than  $T_s'$ , where  $T_s'$  is the synodic period of revolution in the motion of the MPs on fixed initial orbits.

In the case of close approaches between objects (type A), the curves of the orbital elements as functions of time were obtained for various values of  $\varepsilon_r$  – the error of integration on a step – were similar to one another basically up to the first very close approach of the objects. However, the nature and ranges of variation of the orbital elements

were about the same for these curves. Varying  $e_t$  had the same effect on the variations of the orbital elements as variation of the initial positions of the MPs on the orbits.

In the case  $\mu_1 \leq 10^{-5}$  and  $e_0 = 0$ , the maximum eccentricities do not usually exceed  $(7-8) \cdot \mu_1^{1/3}$  when  $\mu_1 \gg \mu_2$  or  $(4-6) \cdot \mu_1^{1/3}$  when  $\mu_1 = \mu_2$  for type A, or  $(4-6) \cdot \mu_1^{1/3}$  when  $\mu_1 \gg \mu_2$  and  $4\mu_1^{1/3}$  when  $\mu_1 = \mu_2$  for type C. When the MPs move inside the Hill sphere, the osculating eccentricities of their heliocentric orbits may be much larger than these values of  $e_{\max}$ . For types A and C, the maximum distance of the MPs from the sun ranged up to  $1 + 1.5\delta$  and  $1 + 2\delta$  when  $\mu_1 = \mu_2 = 10^{-9}$  and to  $1 + 5.6\delta$  and  $1 + 6.6\delta$  when  $\mu_1 = 10^{-5} \gg \mu_2$ .

At large initial eccentricities, the values of  $\beta$  are smaller,  $\gamma$  and  $e_{\max}$  are generally larger, and the  $\alpha$  are almost the same as for smaller values of  $e_1^0$  and  $e_2^0$ . For  $N_i = M$ , the amplitude of the long-period variations of  $e$  may exceed  $e_0$  for certain orientations of the orbits. The results make it possible in some cases (for example, initially circular orbits) to determine the nature and ranges of variation of the orbital elements of two gravitationally interacting objects from the initial data.

The orbits of asteroids that cross the orbit of the earth may vary strongly before they collide with it, with the result that their lifetimes do not depend strongly on the initial orbits.

The author thanks V.N. Zharkov, I.N. Ziglina, and T.M. Éneev for numerous helpful comments.

This study was financed by the National Science Foundation (Grant No. PHY89-04035) in September-October 1992 and by the Russian Fund for Fundamental Research (Grant 93-02-17035) in 1993-1994.

#### LITERATURE CITED

1. A. D. Bryuno, *The Restricted Three-Body Problem. Plane Initial Orbits* [in Russian], Nauka, Moscow (1990).
2. S. I. Ipatov, *Evolution of a Flat Ring of Gravitating Material Points*. USSR Academy of Sciences Institute of Applied Mathematics Preprint No. 2 (1978).
3. S. I. Ipatov, *Mutual Gravitational Effects of Two Protoplanets in the Plane Three-Body Problem with Initially Circular Orbits*. USSR Academy of Sciences Institute of Applied Mathematics Preprint No. 183 (1979).
4. S. I. Ipatov, *The Three-Body Problem and the Interaction of Protoplanets in a Protoplanetary Cloud*. USSR Academy of Sciences Institute of Applied Mathematics Preprint No. 192 (1979).
5. S. I. Ipatov, *Numerical Investigations of the Moments of Inertia of Accumulating Bodies*. USSR Academy of Sciences Institute of Applied Mathematics Preprint No. 101 (1981).
6. S. I. Ipatov, *Certain Questions as to the Origin of the Axial Rotation of Planets*. USSR Academy of Sciences Institute of Applied Mathematics Preprint No. 102 (1981).
7. S. I. Ipatov, "Gravitational interaction of two planetesimals," *Astron. Zh.*, **58**, No. 3, 620-629 (1981).
8. S. I. Ipatov, *Numerical Studies of the orbital evolution of asteroids and planetesimals in the plane three-body problem*. USSR Academy of Sciences Institute of Applied Mathematics Preprint No. 62 (1988).
9. S. I. Ipatov, "Variations of the elements of asteroid-type orbits at 2:5 resonance," *Astron. Vestn.*, **26**, No. 6, 26-53 (1992).
10. S. I. Ipatov, *Gravitational Interaction of Planetesimals Moving on Close Orbits*. Russian Academy of Sciences Institute of Applied Mathematics Preprint No. 23 (1994).
11. R. I. Kiladze, *The Present Rotation of Planets as a Result of the Development of Circumplanetary Swarms of Small Particles* [in Russian], Metsniereba, Tbilisi (1986).
12. A. P. Markeev, *Libration Points in Celestial Mechanics and Cosmodynamics* [in Russian], Nauka, Moscow (1978).
13. L. P. Nasonova, "The Saturn system," *Itogi Nauki i Tekhniki. Ser. Issledovaniya Kosmicheskogo Prostranstva. Dinamika Sputnikov Planet* (ed. E. P. Aksenov), **35**, 70-133 (1991).
14. P. Artymowicz, "Self-regulating protoplanet growth," *Icarus*, **70**, 303-318 (1987).
15. R. Bulirsh and J. Stoer, "Numerical treatment of ordinary differential equations by extrapolation methods," *Numerische Mathematik*, **8**, No. 1, 1-13 (1966).
16. J. Birn, "On the stability of the planetary system," *Astron. Astrophys.*, **24**, 283-293 (1973).
17. S. F. Dermott, "The dynamics of tadpole and horseshoe orbits. I. Theory," *Icarus*, **48**, No. 1, 1-11 (1981).

18. S. F. Dermott, "The dynamics of tadpole and horseshoe orbits. II. The co-orbital satellites of Saturn," *Icarus*, **48**, 12–22 (1981).
19. S. H. Dole, "Computer simulation of the formation of planetary systems," *Icarus*, **13**, No. 3, 494–508 (1970).
20. M. Duncan, T. Quinn, and S. Tremaine, "The long-term evolution of orbits in the solar system: a mapping approach," *Icarus*, **82**, 402–418 (1989).
21. B. Gladman, "Dynamics of systems of two close planets," *Icarus*, **106**, No. 1, 247–263 (1993).
22. B. Gladman and M. Duncan, "On the fates of minor bodies in the outer solar system," *Astron. J.*, **100**, No. 5, 1680–1693 (1990).
23. P. Goldreich and S. Tremaine, "The dynamics of planetary rings," *Ann. Rev. Astron. Astrophys.*, **20**, 249–284 (1982).
24. R. Greenberg, A. Carusi, and G. B. Valsecchi, "Outcomes of planetary close encounters: a systematic comparison of methodologies," *Icarus*, **75**, No. 1, 1–29 (1988).
25. R. Greenberg, W. F. Bottke, A. Carusi, and G. B. Valsecchi, "Planetary accretion rates: analytical derivation," *Icarus*, **94**, 98–111 (1991).
26. Y. Greenzweig and J. J. Lissauer, "Accretion rates of protoplanets," *Icarus*, **87**, No. 1, 40–77 (1990).
27. S. Ida, "Stirring and dynamical friction rates of planetesimals in the solar gravitational field," *Icarus*, **88**, 129–145 (1990).
28. S. Ida and K. Nakazawa, "Collisional probability of planetesimals revolving in the solar gravitational field. III," *Astron. Astrophys.*, **224**, 303–315 (1989).
29. S. I. Ipatov, "Interactions of two bodies moving around the sun," Abstracts of Papers at internationally attended conference on "Theoretical, Applied, and Computational Celestial Mechanics (12–14 October 1993, Sankt-Peterburg), pp. 48–49.
30. S. I. Ipatov, "Dynamics of two interacting objects orbiting the sun," Abstracts of 25th Lunar and Planetary Science Conference (March 14–18, 1994, Houston), pp. 593–594.
31. M. Hasegawa and K. Nakazawa, "Distant encounter between Keplerian particles," *Astron. Astrophys.*, **227**, 619–627 (1990).
32. J. J. Lissauer, "Planet formation," *Ann. Rev. Astron. Astrophys.*, **31**, 129–174 (1993).
33. J. J. Lissauer and M. Kary, "The origin of the systematic component of planetary rotation. I. Planet on a circular orbit," *Icarus*, **94**, 126–159 (1991).
34. S. Mikkola and K. A. Innanen, "Studies on solar system dynamics. II. The stability of earth's Trojans," *Astron. J.*, **100**, No. 1, 290–293 (1990).
35. S. Mikkola and K. A. Innanen, "A numerical exploration of the evolution of Trojan-type asteroidal orbits," *Astron. J.*, **104**, No. 4, 1641–1649 (1992).
36. A. Milani, "The Trojan asteroid belt: proper elements, stability, chaos and families," *Celest. Mech. Dynamic. Astron.*, **57**, 59–94 (1993).
37. A. Milani and A. M. Nobili, "The depletion of the outer asteroid belt," *Astron. Astrophys.*, **144**, No. 2, 261–274 (1985).
38. S. Nishida, "Collisional processes of planetesimals with a protoplanet under the gravity of the protosun," *Prog. Theor. Phys.*, **70**, No. 1, 93–105 (1983).
39. J. M. Petit and M. Henon, "Satellite encounters," *Icarus*, **66**, No. 3, 536–555 (1986).
40. E. Rabe, "Determination and survey of periodic Trojan orbits in the restricted problem of the three bodies," *Astron. J.*, **66**, No. 9, 500–513 (1961).
41. E. Rabe, "Periodic librations about the triangular solutions of the restricted earth-moon problem and their orbital stabilities," *Astron. J.*, **67**, No. 10, 732–739 (1962).
42. V. Szebehely, *Theory of Orbits. The Restricted Problem of Three Bodies*. Academic Press, New York-London (1967).
43. K. Tanikawa, N. Kikuchi, and I. Sato, "On the origin of the planetary spin by accretion of planetesimals. II. Collisional orbits at the Hill surface," *Icarus*, **94**, 112–125 (1991).
44. S. J. Weidenschilling and D. R. Davis, "Orbital resonances in the solar nebula: implications for planetary accretion," *Icarus*, **62**, No. 1, 16–29 (1985).

45. P. R. Weissman and G. W. Wetherill, "Periodic Trojan-type orbits in the earth-sun system," *Astron. J.*, **79**, No. 3, 404-412 (1974).
46. G. W. Wetherill and L. P. Cox, "The range of validity of the two-body approximation in models of terrestrial planet accumulation. II. Gravitational cross-sections and runaway accretion," *Icarus*, **63**, 290-303 (1985).
47. J. Wisdom, "The resonance overlap criterion and the onset of stochastic behavior in the restricted three-body problem," *Astron. J.*, **85**, No. 8, 1122-1133 (1980).
48. Zhang-yin Zhao and Lin Liu, "The stable regions of the triangular libration points of the planets," *Icarus*, **100**, 136-142 (1992).